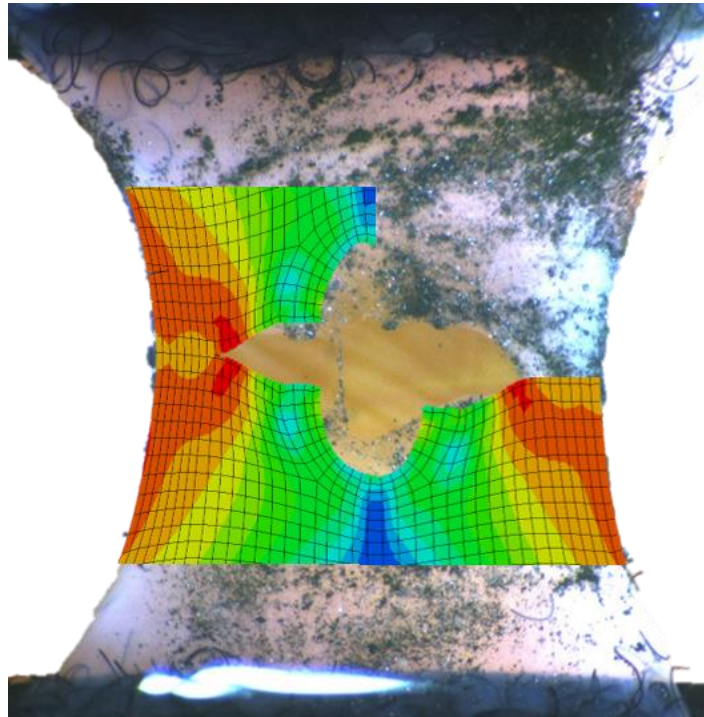


The effects of local fibre organization on the elastic and rupture behaviour of tissue engineered fibrous cap models



Maarten Swaab 4206762

MSc Thesis

Technical University Delft - Erasmus University Medical Center

Supervisor: Dr.ir. Ali C. Akyildiz



Preface

This document contains my thesis to obtain the degree of Master Mechanical Engineering at TU Delft. I performed the required simulations and wrote my thesis as a member of the Biomechanics Laboratory in the Erasmus Medical Centre from August 2020 till August 2021. First I wrote my Literature study, regarding "Modeling Atherosclerotic Plaque Fracture using Tendon Rupture Models". Based on these results, which indicated the importance of collagen fibers on the material properties of collagenous tissues, and the available data from the Biomechanics group, I decided to research the effects of local fibre organisations on the elastic and rupture behaviour on the available samples.

I would like to thank Ali Akyildiz for his guidance in the countless Skype meetings in which we could thoroughly dive into encountered problems. I also want to thank Aikaterini Tziotziou for her feedback and creative ideas. I'd like to thank everyone at the Biomechanics lab for giving me the opportunity to graduate as part of the research group. Finally I want to thank my parents and Sara, who have supported me in every possible way over the years.

Contents

Preface	3
1 Introduction	7
1.1 Atherosclerosis and plaque rupture	7
1.2 Modelling fibrous cap rupture	7
1.3 Tissue biomechanical properties	8
1.4 Aim of the report	8
2 Methods	10
2.1 Material Parameters	10
2.1.1 Bio-engineered tissues	10
2.1.2 Material model	11
2.1.3 Global material parameters	13
2.1.4 Local material parameters	14
2.1.5 Mapping local material parameters to FE models	17
2.2 FEM of uniaxial tensile tests of tissue engineered samples	18
2.3 Modeling tissue rupture using XFEM	20
3 Results	22
3.1 Material parameters	22
3.1.1 Global material parameters	22
3.1.2 Local material parameters	23
3.1.3 Mapping local material parameters to FE models	26
3.1.4 Effects local material parameters on stress-strain curve	27
3.2 FEM of uniaxial tensile tests of tissue engineered samples	28
3.3 Modeling tissue rupture using XFEM	33
4 Discussion	37
4.1 Material parameters	37
4.1.1 Material model	37
4.1.2 Global material parameters	37
4.1.3 Local material parameters	39
4.1.4 Mapping local material parameters to FE models	39
4.2 FEM of uniaxial tensile tests of tissue engineered samples	40
4.3 Modeling tissue rupture using XFEM	41
4.3.1 Lessons learned regarding XFEM	43
4.4 Recommendations	43
5 Conclusion	46
Appendix A	48
Appendix B	59
Appendix C	65
References	79

Abstract

Atherosclerosis is a cardiovascular disease in the arteries and a primary cause of death in the industrialized world. Most deaths due to atherosclerosis occur when the fibrous cap covering the necrotic core ruptures, leading to a blood clot. To determine whether an atherosclerotic plaque will rupture requires the development of accurate computational models. One of the key aspects for these models is the material model, in which collagen fibres play a major role. This study aims to contribute to the making of a numerical model which accurately represents atherosclerotic plaque by comparing the elastic and rupture behaviour of engineered collagenous micro tissues and their respective finite element models in ABAQUS.

The Holzapfel-Gasser-Ogden material model of these computational models is based on a combination of global material parameters and local material parameters based on the local fibre organisation. A framework developed to measure the local fibre organisation using provided imagery of a nuclear stained tissue engineered sample shows the collagen fibres align along the loading direction and the edges of the geometry. The fibers are less dispersed along the edges of the geometry and on the left and right of a formed soft inclusion.

A uniaxial tensile test was performed on four tissue engineered samples. The elastic and rupture behaviour of the samples during the uniaxial tensile tests is replicated in ABAQUS using both isotropic and homogeneous material parameters, and anisotropic heterogeneous material parameters. The stresses measured in the simulations are highly dependent on both the material parameters and the geometry of the model. The strains are mostly dependent on the geometry, but are affected by the material model. Due to the higher stiffness at the edges of the geometry of the anisotropic samples, the stresses increased greatly, and the strains decreased slightly.

The rupture behaviour of the cultured samples is replicated in the FEM simulations using extended finite element method (XFEM). The damage in the samples with isotropic material parameters initiates both from the soft inclusion as the left and right edges of the geometry. The damage in the samples with anisotropic material parameters initiates, similarly to the cultured samples, only from the sides of the soft inclusion. The damage in both the cultured and simulated samples propagate mostly horizontal and from the soft inclusion outward. In three out of four isotropic samples however, damage propagates to varying degrees from the edge of the geometry inward.

Based on these findings it is concluded that implementing the local fibre organisation in the material model can improve the accuracy of finite element simulations of collagenous soft tissues, which includes atherosclerotic plaque, as the rupture behaviour of the simulations with anisotropic material parameters more accurately represents the rupture behaviour of the engineered fibrous tissues in comparison with simulations with isotropic material parameters.

1 Introduction

1.1 Atherosclerosis and plaque rupture

Atherosclerosis is a cardiovascular disease in the arteries and a primary cause of death in the industrialized world[1]. It is caused by the accumulation of inflammatory cells and low density lipoproteins (LDL) inside the intimal part of the arteries. Over the years of a human life, this accumulation leads to a necrotic core in the vessel wall, which is separated from the lumen by a fibrous cap, as illustrated in Figure 1. This fibrous cap is a distinct layer of connective tissue completely covering the lipid core[2]. Around 15 percent of heart attacks are due to lumen stenosis; the plaque restricting the lumen, and restricting blood flow. Most heart attacks however are due to the fibrous cap rupturing, leading to the development of a blood clot, as can be seen in Figure 1, which can lead to thrombosis[3].

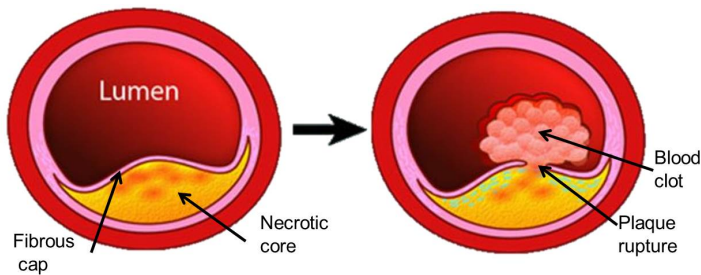


Figure 1: Rupture of the fibrous cap, leading to the necrotic core to form a blood clot in the lumen[1].

Whether a fibrous cap ruptures depends on two factors; the geometry and material properties of the fibrous cap and the necrotic core. When reviewing the relationship between the geometries and dimensions of the plaque and fibrous cap, there is a general consensus that a fibrous cap has a higher likelihood to rupture when the necrotic core is relatively large, and the fibrous cap is relatively thin[4]. Such a plaque does not necessarily rupture however[5]. Therefore it would bring unnecessary risk to treat all found plaques. Whether the plaque ruptures also depends on many biological factors, which alter its material properties. One of the key parameters regarding the mechanical properties of the fibrous cap is the stiffness and architecture of collagen fibres within the fibrous cap[5],[6].

1.2 Modelling fibrous cap rupture

One of the primary goals of research fields regarding atherosclerosis is to develop a way to systematically and quantitatively predict the behaviour of atherosclerotic plaques, which includes its rupture behaviour. The data required for this research is difficult to acquire. This is due to atherosclerosis being a progressive disease which evolves over several decades, where real-time human in-vivo measurements are difficult to perform. This is where computational simulations come into play, as they could allow the prediction of the rupture of plaques, or

could give an indication what the impact of different biomechanical parameters is on the rupture behaviour of atherosclerotic plaque[7]. Four groups of input parameters are required for computational models. These four groups are the forces acting on the plaque, the geometry and the material properties of all parts of the plaque and the boundary conditions of the system[6].

Finding the material properties of atherosclerotic plaque tissue presents several challenges. The tissue is often too small to handle, the shapes of the plaques are irregular, and the tissue is highly heterogenous[8]. Besides that is the fact that human tissue samples are hard to acquire, and mechanical in-vivo testing is almost impossible. Therefore bio-engineered tissues can be used as a simplified, available and more controlled substitute of plaque tissue. In this thesis, we will make use of four tissue engineered fibrous cap models[9]. These collagenous micro tissues were produced to systematically investigate the relationship between material contents and tissue mechanics. The results from the uniaxial tests of these collagenous micro tissues were provided by the Erasmus MC. In this research, the collagenous micro tissues are referred to as cultured samples.

1.3 Tissue biomechanical properties

There are many biological aspects of biological tissue which alter its mechanical properties. As a model is by definition a simplified version of real tissue, it is critical to decide what aspects should be taken into consideration when making a model, and how to represent these biomechanical aspects using mathematical formulas. Arterial tissue falls under the category of soft tissues. They are characterized by their composite structure, consisting of mostly type 1 Collagen, a well-hydrated extra cellular matrix and other cells.

Collagen is the main load bearer of the tissue[10]. The contribution of collagen to the stiffness of the tissue depends on the stiffness of individual fibres, their distribution, amount and the cross-links between fibres. In general, the higher amount of fibres in the direction of the load, and the more fibre crosslinks, the stiffer the tissue. Besides collagen, smooth muscle cells, elastin and calcifications can also play a large role in determining the biomechanical properties of the fibrous cap, depending on the type of atherosclerosis. What is clear however, is that atherosclerotic tissue is highly heterogenous and anisotropic[6].

1.4 Aim of the report

This thesis aims to generate numerical models that can accurately capture the mechanical behaviour of tissue engineered fibrous cap models, to ultimate contribute to a numerical model which accurately predicts atherosclerotic plaque rupture. This is done by comparing the elastic and rupture behaviour of collagenous micro tissues and their respective finite element models. Within this scope, the focus will be on the effects of local collagen distribution within the tissue engineered fibrous cap model on their mechanical properties. First a workflow is presented on how the tissue could be modelled; what material model is used, what parameters it requires, and how these parameters can be determined. This model is then incorporated in finite element software to simulate the elastic and rupture behaviour of the models, where a comparison is made between an isotropic and an anisotropic version of the finite element model. Finally the rupture behaviour of the two versions of the computational models

is compared to the rupture behaviour of the uni-axially tested samples. This leads to the following research question for this thesis: "What are the effects of local collagen fibre organisation on the elastic and rupture behaviour of a tissue engineered fibrous cap model?"

2 Methods

The method section consists of three sections. First is a description of the methodology used to find the required inputs for the used material model in the computational models. Second is the methodology regarding the replication of the uniaxial tensile tests of the cultured samples in ABAQUS. Third is the methodology used to model the rupture behaviour of the computational models using the extended finite element method (XFEM).

2.1 Material Parameters

2.1.1 Bio-engineered tissues

The micro tissues provided by the Erasmus MC were created by culturing myofibroblasts in fibrin-based gels and treated to cell culture protocols. These protocols contained the exposure of the samples to either dynamic loading or no loading. The four cultured samples regarded in this study are shown in Figure 2.

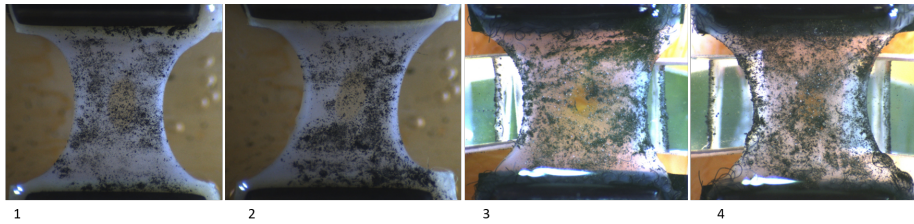


Figure 2: Four tissue engineered collagenous micro tissue samples which underwent uniaxial tensile testing. A soft inclusion is added in the middle of the samples. The samples are 8 to 12 mm in length and on average 0.6 mm thick.

A soft inclusion (SI) was created in the middle of each tissue to mimic a necrotic core, which is separated from the lumen by a fibrous cap, as shown in Figure 3.

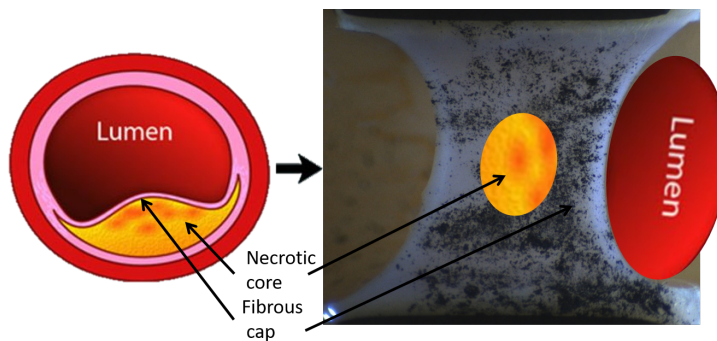


Figure 3: The tissue engineered collagenous micro tissue samples were cultured with a geometry to represent the fibrous cap of atherosclerotic plaque. The soft inclusion mimics the necrotic core, the lumen is on the sides of the tissue, and the two are separated by a fibrous cap[1].

The micro tissue mechanics of the cultured samples was determined by uniaxial tensile tests after 21 days of culturing. During these tests the force-displacement curves were measured. Videos of the cultured samples undergoing the uniaxial tensile test were converted to pictures at a frequency of 15 Hz, which allowed for the visualization of the elastic and rupture behaviour of the samples under load. Both the force-displacement curves and images were provided by researchers from the Erasmus MC.

Of all the samples that tensile tests were performed on, eight had their rupture in the inclusion site, rather than where the samples were clamped. Out of these eight samples, four were in the group that was not exposed to loading during the culturing. These four samples showed a significantly more isotropic fibre distribution in comparison with their dynamically cultured counterparts[9]. Therefore these four samples were not taken into account, leading to 4 cultured samples regarded in this study.

2.1.2 Material model

Based on the data available; force-displacement curves and images, the material model used must be a mostly phenomenological one. Biological tissues are often modelled with hyperelastic material models, as these tissues are non-linearly elastic. Visco-elasticity was not taken into account, due to the slow strain rate of the experiments, which should minimize the visco-elastic effects. The phenomenological material model should however take into account the local fibre organisation. Therefore the extensively used Holzapfel Gasser Ogden (HGO) model was chosen[11],[12].

This phenomenological material model, which also requires structural information based on histology, was designed to model arterial layers. It allows for the contribution of an isotropic hyperelastic extracellular matrix and the anisotropic contribution of collagen fiber families. In the HGO model specifically, the anisotropic contribution not only depends on the amount of fibres, but also on the fibre orientation and dispersion. This allows for the development of a free-energy function which takes this collagen fibre data into account. A visualisation of the different input parameters for the HGO model is given in Figure 4.

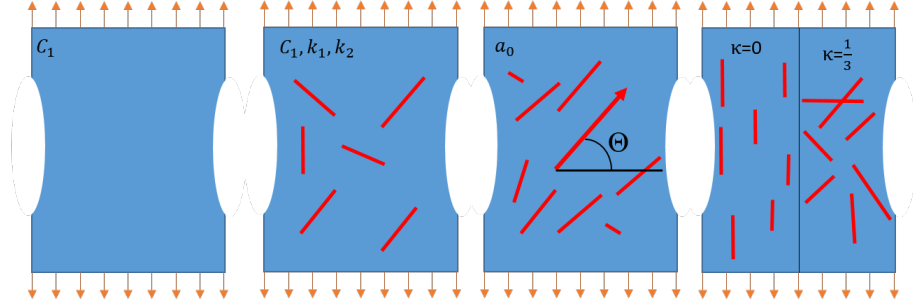


Figure 4: Representation of the input parameters for the HGO model, where C_1 is required for the strain energy of the isotropic EMC. k_1 and k_2 are parameters regarding the collagen fibers. a_0 represents the mean fibre angle of a set group of collagen fibers. κ gives the collagen fibre dispersion for a set group of collagen fibers.

The deformation gradient F of the material leads to the right Cauchy-Green tensor, denoted C . The Helmholtz free-energy function Ψ , or strain energy, is based on C and the material model of the tissue.

To get only the isochoric contribution of Ψ , a purely volumetric contribution $U(J)$ is separated from the strain energy function. Only the isochoric contribution of Ψ , $\bar{\Psi}$, is regarded, based on the assumption of incompressibility of the tissue.

$$\Psi(C, A_1, A_2) = U(J) + \bar{\Psi}(\bar{C}, A_1, A_2) \quad (1)$$

Where \bar{C} is the deviatoric component of the right Cauchy-Green tensor, and A_1 and A_2 are two symmetric second-order tensors which describe the anisotropic and hyperelastic stress response of arterial tissue. Based on the isochoric contribution of the strain energy, the deviatoric component of the second Piola-Kirchhoff stress \bar{S} can be calculated.

$$\bar{S} = 2 \frac{d\bar{\Psi}(\bar{C}, A_1, A_2)}{d\bar{C}} \quad (2)$$

Based on this the stiffness matrix \bar{K} , which is necessary for the Finite Elements model, can be calculated[13].

$$\bar{K} = 2 \frac{d\bar{S}}{d\bar{C}} \quad (3)$$

The deviatoric component of the strain energy $\bar{\Psi}$, consists of two components; a deviatoric isotropic component $\bar{\Psi}_{iso}$ and a deviatoric anisotropic component $\bar{\Psi}_{ani}$.

$$\bar{\Psi} = \bar{\Psi}_{iso} + \bar{\Psi}_{ani} \quad (4)$$

The strain energy of the deviatoric isotropic matrix is based on the incompressible isotropic neo-Hookean model

$$\bar{\Psi}_{iso} = 0.5C_1(\bar{I}_1 - 3) \quad (5)$$

where $\bar{I}_1 = tr(\bar{C})$ and C_1 denote the first invariant of \bar{C} and the neo-Hookean parameter respectively. The anisotropic collagen fibre part of the strain energy

$\bar{\Psi}_{ani}$ in the mean fibre direction a_0 is calculated by

$$\bar{\Psi}_{ani}(\bar{C}, H) = \frac{k_1}{2k_2} [\exp(k_2[\kappa\bar{I}_1 + (1 - 3\kappa)\bar{I}_4 - 1]^2) - 1] \quad (6)$$

Where the k_1 is a stress-like parameter and k_2 is a dimensionless parameter. Both parameters are determined per sample using mechanical tests. I_4 is a tensor invariant equal to the square of the stretch in the direction of a_0 . \bar{I}_1 is the first invariant of \bar{C} . The κ is the fibre dispersion within a family of fibres, and can together with the mean fibre direction a_0 be measured based on imaging techniques applied to the sample tissue. H is the generalized structure tensor dependent on κ and a_0 . The fibre dispersion is based on the fibre density function $\rho(\Theta)$ and the Eulerian angle Θ by

$$\kappa = \int_0^\pi \rho(\Theta) \sin^3(\Theta) d\Theta \quad (7)$$

The density function is normalized using

$$\int_0^\pi \rho(\Theta) \sin(\Theta) d\Theta = 2 \quad (8)$$

The von Mises distribution of the collagen fiber density at different κ is shown in Figure 5. As shown in the figure, the κ is 0 for full fibre alignment, and 1/3 for complete dispersion.

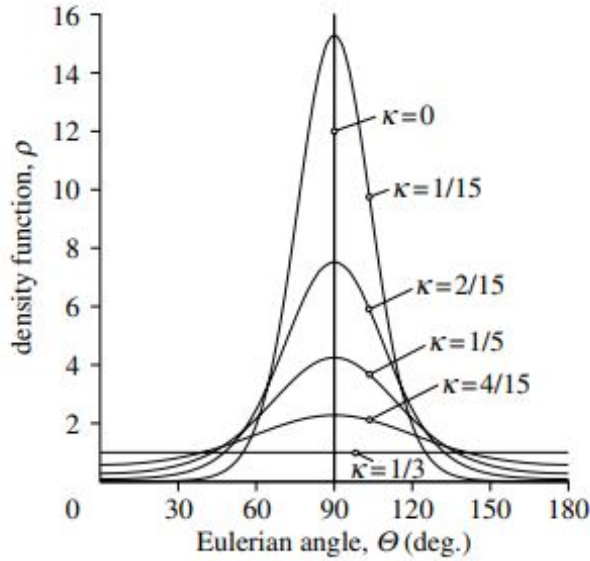


Figure 5: Two-dimensional graphical representation of the von Mises distribution of the collagen fibers[11].

2.1.3 Global material parameters

The five material parameters required for the HGO model, C_1 , k_1 and k_2 , a_0 and κ are subdivided into two groups; global and local material parameters. The

global material parameters are equal within one sample. The local material parameters differ depending on the location within one sample. The distinction on whether a parameter is global or local is based on the available data regarding the tissue engineered samples. The material parameters assumed global in this research, C_1 , k_1 and k_2 , are based on one sample out of four and are assumed equal for all four samples.

The surface geometry of the cultured sample used to find the global material parameter at the start of the tensile test is traced in the xy plane of a three-dimensional ABAQUS/Standard (Dassault Systems) model, as shown in Figure 6. The thickness of the model was set at the average thickness of the cultured sample at 0.6 mm. The global parameters were manually varied to replicate a force displacement curve of the elastic part of the tensile test of the sample in the simulation. The bottom of the sample was fixed, and boundary condition in the form of a ramp displacement in y direction was applied to the top of a single element connected to the top of the sample.

The reaction force measured was based on the stresses in yy direction and the surface in the xz plane in a single element connected to the top of the simulated tissue. The tissue was assumed completely homogeneous and incompressible. The sample was set to have isotropic material parameters, by setting the ν at $\frac{1}{3}$.

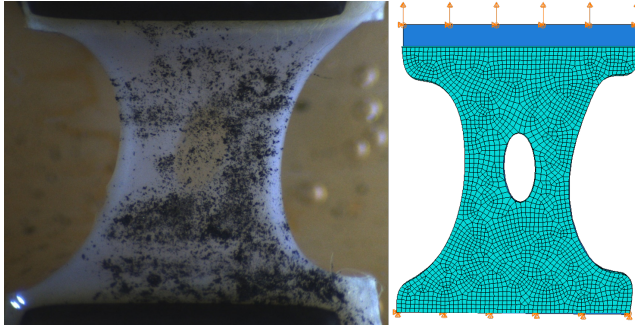


Figure 6: The silhouette of an image of cultured sample 2 before the uniaxial tensile test begins (left) is replicated in ABAQUS (right).

2.1.4 Local material parameters

The collagen fibre organisation of the bio-engineered tissues could be visualized using nuclear stain and an in house developed probe. For this study only one sample with staining was available, which is shown in Figure 7. When referring to this nuclear stained sample in this document, the term stained sample is used. It is part of the group that endured intermittent dynamic loading during culturing, but was not included in the uniaxial tensile tests. High detail images at different depths of this one stained sample were provided by researchers from the Erasmus MC.

The local mean fibre direction a_0 and fibre dispersion κ based on the stained sample are measured and calculated over a specific part of the area of the tissue to create local material parameters per part of the area. To subdivide the total image into smaller images, the silhouette of the stained sample was replicated

in ABAQUS. Here the nodal coordinates were used to create separate images per ABAQUS element using a Matlab script, as shown in Figure 7. The Matlab script is provided in Appendix A. The ABAQUS model was meshed at two densities, leading to 94 and 245 elements and images to ensure that the mesh density had negligible effect on the local material parameter results.

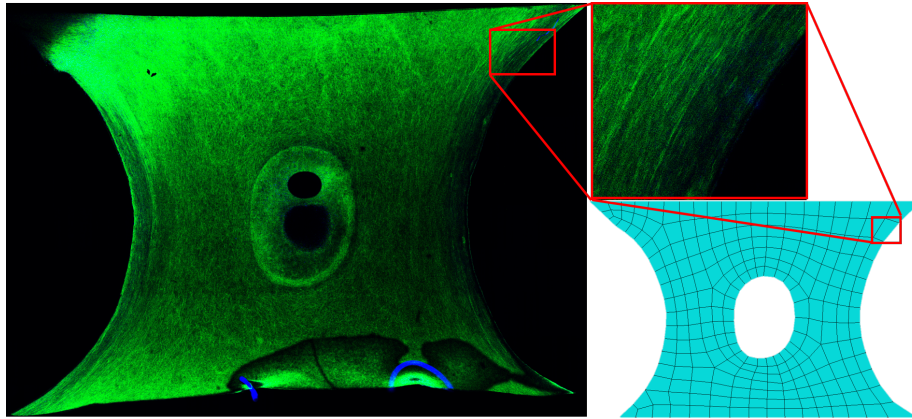


Figure 7: Cultured sample that is nuclear stained (left) to display collagen fibres. It is divided into smaller images (top right) for which the local fibre organisation is measured. The size and position of these smaller images is based on the coordinates of the nodes in the ABAQUS input file (bottom right). The geometry of the ABAQUS input file replicates the silhouette of the cultured stained sample.

Furthermore, the images of the tilescan were taken at three different depths into the tissue, to ensure that the depth would have limited effect on the results. The lighting of the image could be altered in the post processing tool Las X (Leica Microsystems). The tool could only lead to the proper lighting of around half of the tissue however. Therefore for each depth the region that was lit properly was altered. At $105 \mu m$, the right side was lit properly, at $119 \mu m$ the total image could be lit properly, and at $135 \mu m$ the left side was focused on. The three images at the different depths of the stained sample used for the calculation of the local fibre organisation are shown in Figure 8.

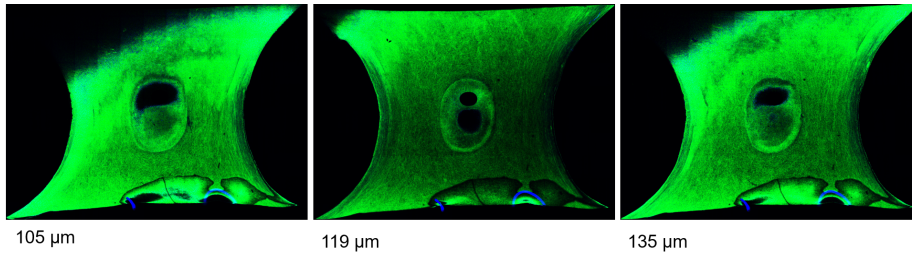


Figure 8: Cultured sample that is nuclear stained to display collagen fibres. Images were taken at three different depths to ensure the depth of the image had negligible effects on the measuring of the local fibre organisation. The depth at which the picture is taken is given below the image.

To determine the mean fibre angle per smaller image, the open-source collection of Matlab scripts FibLab was used[14]. FibLab allows for the extraction of fibres and their angles based on the differences in colouring within the provided images. Based on these fibre angles per image, FibLab calculates the peak fibre angle. Using FibLab rather than calculating the mean fiber angles using a normal distribution has two major advantages. Firstly FibLab is able to take the isotropic fraction of the fibers into account, which allows for a more accurate peak centre angle, as it filters out this isotropic fraction. The second advantage is that FibLab takes the wrapping of the angle data into account. A regular normal distribution from 0 to π does not take wrapping into account, which will often lead incorrect results, as shown in Figure 9. Therefore, the peak fibre angle as described by the FibLab documentation[14] instead of the mean fibre angle as described in the HGO model [11] is used as the input for a_0 .

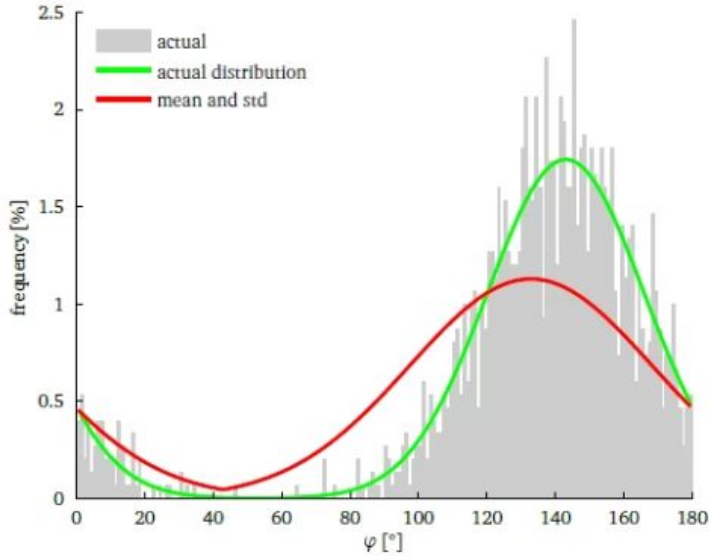


Figure 9: Histogram of angles. The red line shows the normal distribution with a mean μ and standard deviation σ . The green shows the results based on the calculations in FibLab. It shows the importance of wrapping, as the μ is off due to the small peak at $\phi = 0$ degrees.[14]

The fibre dispersion is calculated based on the same found angles per element used for the peak fibre angle. The angles θ required for κ are the angles of each fibre relative to the peak angle. These relative angles are grouped together in 180 bins, where every one degree is a bin. The weight of these bins is normalized using the density function of equation 8. The κ is then calculated with equation 7 per image and element.

As stated previously, the stained sample could be photographed at different depths, of which three were chosen based on the quality of the images. To minimize measuring errors of individual small images, the three different depth based datasets were combined into a single dataset. For each smaller image the sample depth, and thus datapoint was selected based on what datapoint had the highest amount of angles found by FibLab. It was assumed that a higher angle count would lead to a higher accuracy.

2.1.5 Mapping local material parameters to FE models

The four cultured samples analyzed in this study, which were mechanically tested under uniaxial testing conditions, have a geometry generally similar to the stained sample shown in Figure 7. To average the local fibre orientation and dispersion from the stained sample, the different data points were grouped together into subregions by using partitions of the part in ABAQUS. This was done to filter out local errors in the data from the tilescan, as it will lead to more generalized outputs. These subregions were given local material parameters in the simulations of the four samples. By using partitions in the part, the element groups could be easily identified in the ABAQUS input file. This allowed for the assigning of local material parameters. The κ and a_0 were both taken into

account in combining elements together to create the element subgroups, with the objective to minimize the differences in material parameter values within one subgroup. The way to mathematically implement these groups into ABAQUS was also considered when dividing the groups. Only the top right quarter of the data from the stained sample was used, as it most clearly shows the fibre orientation and dispersion of the stained sample. An assumption was made that the local material parameters were symmetrical for all four quarters of the samples.

2.2 FEM of uniaxial tensile tests of tissue engineered samples

The uniaxial tensile testing of the four cultured tissues is replicated using the commercial Finite Element Software ABAQUS/Standard (Dassault Systems). When referring to these ABAQUS simulations the term "simulated samples" is used. To simulate the hyperelastic behaviour of the four samples, the four requirements for a simulation: geometry, forces, boundary conditions and material model were implemented in ABAQUS. The silhouette of the geometry of the four samples is based on images taken during the start of the tensile test. Since only 2D fibre data is available, the tissue is modelled as a 2D geometry, as shown in Figure 10. No force boundary conditions are applied, as the experiments are displacement driven uniaxial tensile tests. Two boundary conditions are applied. First the bottom of the mesh is constrained for x and y displacement and for rotation around the z-axis. These constraints are based on the clamping of the cultured tissues, which should keep the tissue from displacement in any direction and should resist rotation around z. The x displacement and rotation around z are also bound in the top of the mesh. The y displacement increases over simulation time as a ramp where the maximum displacement is set at around twenty percent above the displacement at which the cultured samples completely ruptured.

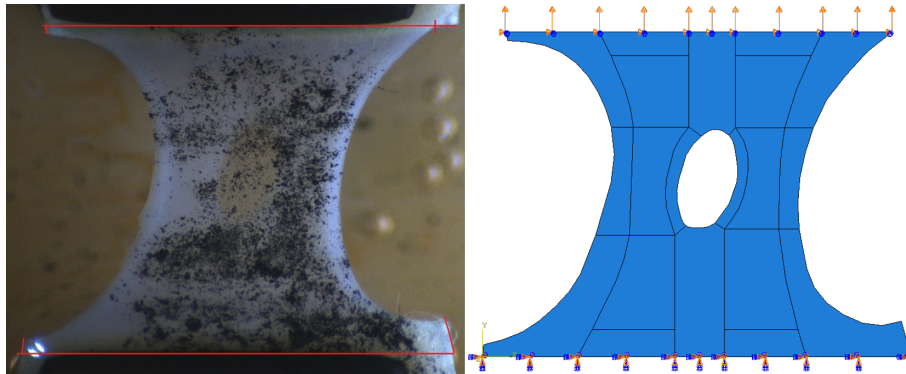


Figure 10: Sample 2 at the start of the uniaxial tensile test (left) is replicated in an ABAQUS model (right). The partitions in the ABAQUS model allow for the implementation of local material parameters per subgroup. The x and y displacements and rotation around z are bound at the bottom of the part. The x displacement and rotation around z are bound at the top. The y displacement at the top increases over time to replicate the uniaxial tensile test.

To measure the effect of implementing local fibre organisation on the hyperelastic behaviour of the four simulated samples, two simulations were done per cultured sample. An isotropic version where the κ was set at $\frac{1}{3}$ and an anisotropic one where the κ and a_0 were set locally based on the results from Chapter 3.1.2. The local material property groups shown in Figure 16 are applied in the ABAQUS simulations using partitions in the sketch of the geometries. Symmetry is applied for all four quarters of the sample regarding the κ and a_0 . To visualize this, the fibre orientation and dispersion for sample four is shown in Figure 11. Though the local material parameters are assumed symmetrical, the actual geometry of the samples is not.

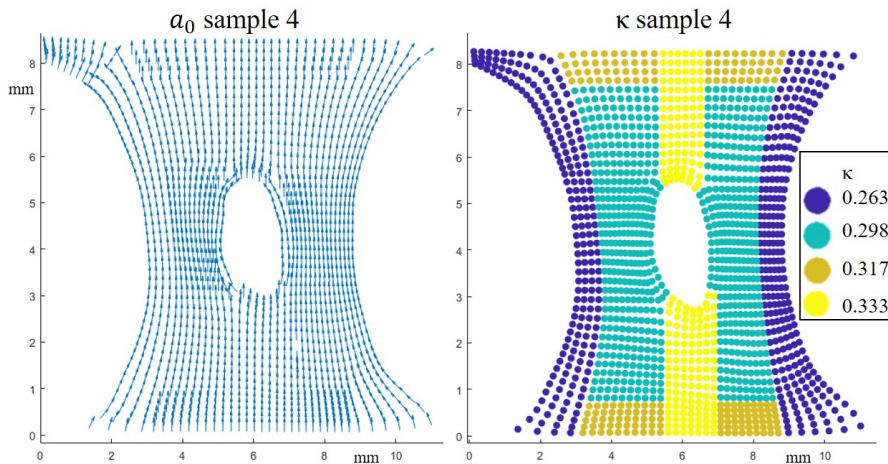


Figure 11: Fibre orientation (left) and dispersion (right) implemented per element in sample 4.

The elastic responses of the isotropic and anisotropic samples are compared based on the amount and location of the maximum principal stresses and strains measured. Throughout this document, stresses and strains refer to maximum principal stresses and strains, unless stated otherwise. Furthermore, the stresses and strains of regions that are relevant regarding rupture initiation are compared per region over time.

The elements are of type CPS4R, which are 2 dimensional elements with 4 nodes from the plane stress family with reduced integration and hourglass control. The reduced integration scheme was chosen for computational efficiency. Furthermore, due to the non-linearity of the material, a reduced integration scheme is recommended[15]. The analysis step was set as a geometrically non-linear one. Automatic stabilization is applied based on the dissipated energy fraction, set at a standard value of 0.0002, and an adaptive stabilization with a maximum ratio of stabilization to strain energy of 0.05. A maximum number of increments was set at 100000, with an initial and maximum step size of 0.01 sec, and a minimum of 1E-08 sec. The step size is automatically determined by ABAQUS. The simulations were set as discontinuous analysis. This leads to the number of equilibrium iterations after which the check is made whether the residuals are increasing in two consecutive iterations double from 4 to 8, and

the number of consecutive equilibrium iterations at which logarithmic rate of convergence check begins is increased from 8 to 10. The elements are purely quadrilateral elements, and the mesh is based on the medial axis with minimized mesh transition.

In Finite Element modelling there is a trade off between computation time and accuracy. This trade off is determined by i.a. the mesh density. To minimize the computation time, a test was done regarding two different mesh densities, and the effect this had on the hyperelastic stress and strain results. The isotropic version of sample 4 was meshed with 1587 and 6107 elements.

2.3 Modeling tissue rupture using XFEM

To represent the failure of the sample tissue, the extended finite element method (XFEM) was implemented in the ABAQUS simulations. XFEM allows for the study of crack initiation and propagation, as it does not require the user to define a crack path. XFEM also allows the use of the workflow presented for local fibre orientation and dispersion as XFEM does not require remeshing during crack propagation. It is based on the concept of partition of unity[16]. Cracks create discontinuity in the functions that are used to approximate displacement in finite elements. With XFEM, local enrichment functions and additional degrees of freedom are added to nodes near the crack. The gap between nodes created by the crack is represented by a discontinuous function.

The goal of implementing XFEM to the simulations was to replicate the rupture behaviour of the cultured samples during the uniaxial tensile tests. To match the rupture behaviour of the isotropic and anisotropic versions of the four simulated samples, the input parameters of XFEM in ABAQUS were iteratively changed to get a matching result.

XFEM requires several inputs, of which the used values during the simulations are given in Table 1. First is the region where damage might occur; the crack domain. As the crack should occur left and right of the soft inclusion, the subgroups which include this part of the sample were set as the crack domain. These were subgroups 1, 2 and 3, which are visualized in Figure 16.

Second is the damage initiation threshold. It is based on either max principal stress or max principal strain per element set by the user. XFEM will not be part of the simulation until one element reaches that threshold. Based on the location of high stresses and strains shown in Chapter 3.2, is the threshold set at a maximum principal strain. The damage initiation strain threshold is equal to the maximum strain measured in an element at a displacement in the simulation equal to the displacement of rupture initiation in the cultured samples. This ranged between 30 and 40 percent max principal strain, depending on the sample. The maximum strain damage initiation threshold was set at 30 percent, as setting a higher threshold lead to immediate divergence issues in the simulations.

Next is the damage evolution parameter, which is based on a set Fracture energy. The amount of fracture energy was manually iterated per simulation to ensure a maximum crack propagation. Third is the viscosity coefficient, which aids in the stability of the stimulation. The viscosity coefficient value was iteratively determined to ensure a maximum crack propagation with values ranging between 0.001 and 0.0001.

Table 1: XFEM input parameters per sample for the isotropic (iso) and anisotropic (ani) versions of the simulations

Sample	Max Strain	Fracture Energy	Viscosity Coef
1 iso	0.3	0.15	0.001
1 ani	0.3	0.08	0.001
2 iso	0.3	0.2	0.0001
2 ani	0.3	0.15	0.001
3 iso	0.3	0.2	0.001
3 ani	0.3	0.5	0.001
4 iso	0.3	0.1	0.001
4 ani	0.3	0.1	0.001

3 Results

3.1 Material parameters

3.1.1 Global material parameters

After ten iterations of manually changing the parameters C_1, k_1 and k_2 , the global material parameters were set at the values shown in Table 2.

Table 2: Global material parameters used in the ABAQUS simulations based on the replication of uniaxially tensile tested sample 2.

Parameter	Value	Unit
C_1	0.05	MPa
k_1	26	MPa
k_2	2.5	

These global material parameter values lead to the following reaction forces at the top of the sample at different displacements in ABAQUS, as shown in Figure 12. The starting length of both the cultured and simulated sample is 12.16mm. Both the experimental and simulated force displacement curves show distinct hyperelastic material behaviour. At low displacement there is for both a clear toe region, where in the cultured samples the collagen fibres uncoil and are recruited to start bearing load. At a displacement of around 1.2 mm the collagen fibres are recruited, and the linear part of the force displacement curve begins. The force displacement curve of the simulated sample shows less of a linear part, and more of a continual rise of the force derivative. At around 2.4 mm, the derivative of the force displacement curve of the experimental results starts to decrease, which indicates the beginning of damage in the cultured tissues. The force displacement curve of the simulated sample however keeps increasing, as no damage is modelled. Therefore the maximum displacement in the simulation was set at 2.4mm. The comparison of force displacement values between the simulated and cultured sample over time in the toe region and the start of the linear region leads to an RMSE of 0.0189 mN and a relative mean error of 47 percent over the length of the first 1.06 mm. The simulated sample eventually has a steeper slope at higher displacements, leading to an RMSE of 0.0441 mN and a relative error of 24.8 percent over the total curve.

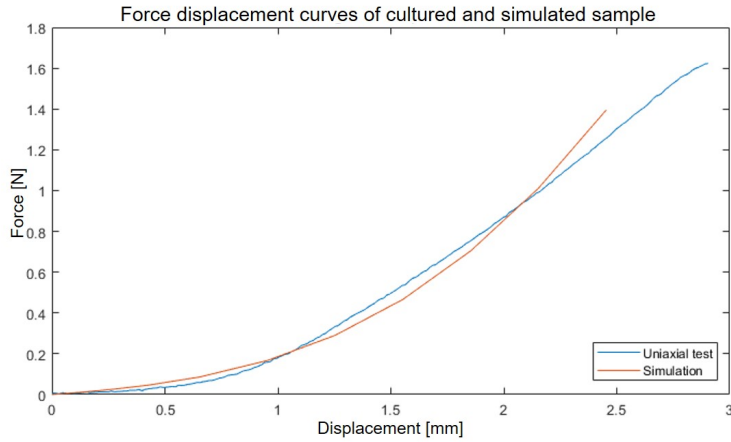


Figure 12: Force displacement curves of the cultured sample under uniaxial tensile testing conditions (blue) and the simulation which replicates the experimental results (red). The curve from the simulated sample uses the global material parameters from Table 2 to replicate the experimental results of the cultured sample.

3.1.2 Local material parameters

The Fiblab calculations regarding the peak fibre angle per element, combined with the coordinates of the centre of each element is visualized in Figure 13. The left three graphs show the peak fibre angle of the 94 elements, the right three graphs show the a_0 of the same stained sample, but divided in 245 elements. On the left and right side of the inclusion, there is a trend in the angles which follows the curvature of the left and right edge of the tissue. Above and below the inclusion however there is a much more distorted angle distribution. Another part of the tissue which seems highly unorganised is the top left of the sample, where the amount of distorted elements changes per depth. Finally there seems to be a distortion of the peak fibre angles in the bottom right of all six samples. When comparing the peak fibre angles at the same depths but with different mesh densities, it is clear that the differences between them are negligible.

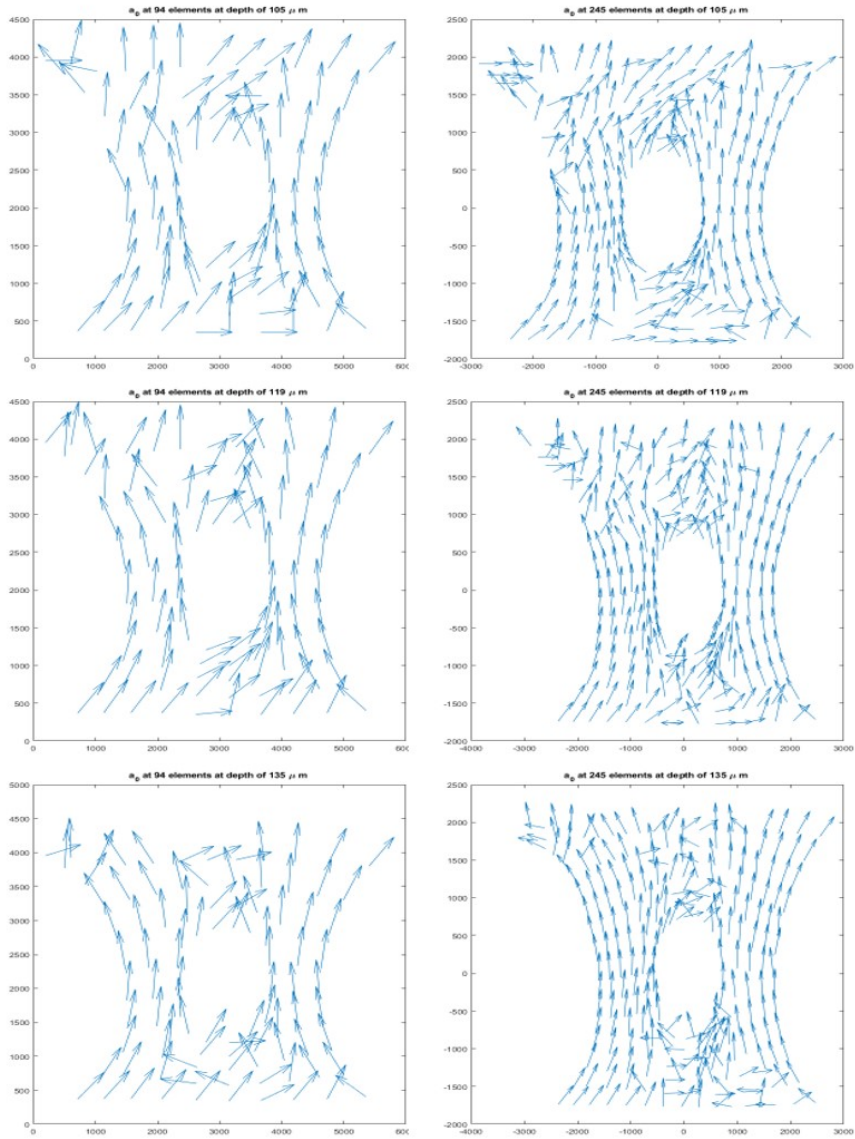


Figure 13: Local peak fibre angles measured in the stained sample using FibLab regarded at three depths, with mesh densities of 94 (left) and 245 elements (right). The x and y axis are the pixels of the images of the nuclear stained sample.

To calculate the κ , the three image depths and two mesh sizes leads to six different fibre dispersion datasets, which are visualized in Figure 14. The left three graphs show the fibre dispersion of each of the 94 elements at three different depths in the tissue, the right three graphs show the fibre dispersion for all 245 elements, at those same three depths. When comparing the different depths with the same amount of elements, it is clear that at 105 μm the fibres

at the sides of the tissue are more aligned at the right side of the tissue, at $119 \mu m$, they have generally similar fibre dispersions at both sides, and at $135 \mu m$, the left side has a lower κ . Furthermore, the κ left and right of the soft inclusion is generally higher than the κ above and below the soft inclusion. The differences in κ between different mesh densities are negligible.

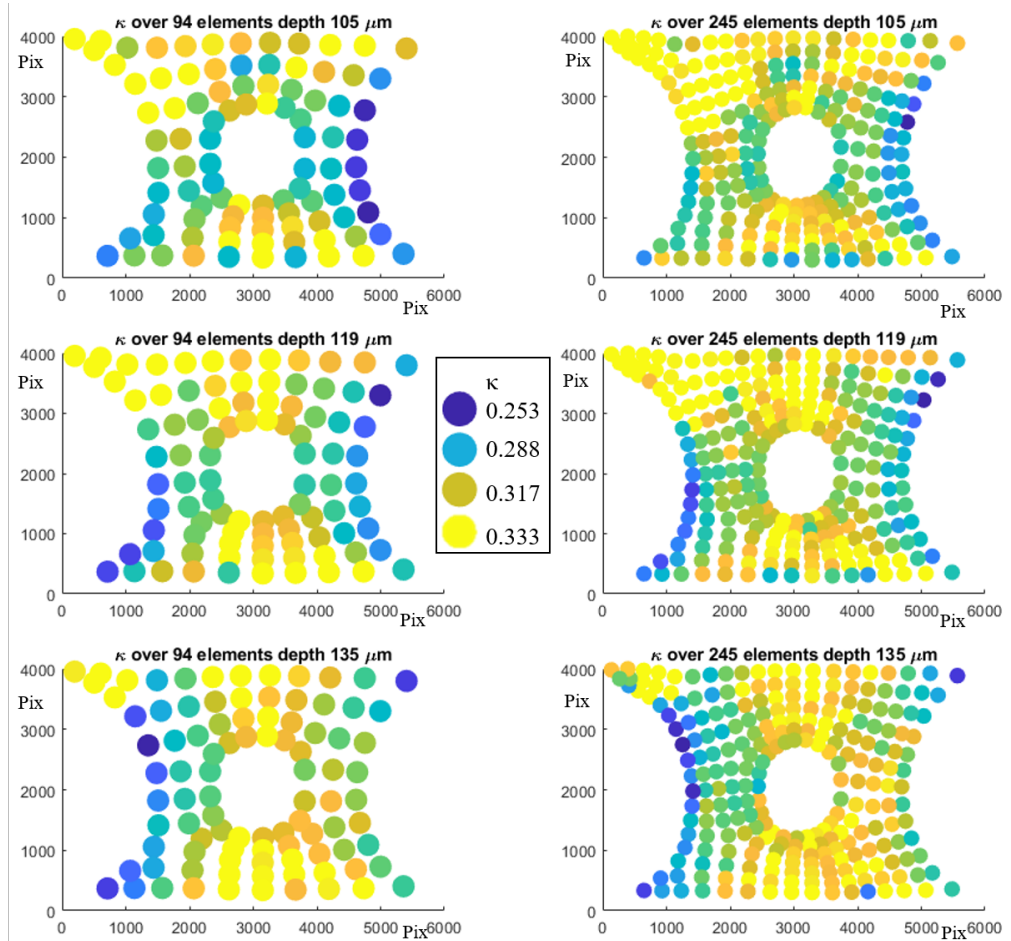


Figure 14: The local κ of the tilescan at three depths, at two element mesh densities. The x and y axis are the pixels of the images of the nuclear stained sample.

Combining the κ and a_0 data sets of the three image depths for the two mesh sizes, by choosing the element per depth with the most angles found by FibLab, leads to the results shown in Figure 15. In this plot the direction of the red arrow shows the peak fibre angle per element. The size of the arrow shows the degree of fibre dispersion. The more dispersed, the smaller the arrow. The dispersion is further displayed by the colored circles, where a more blue circle equals an element with a lower κ , and a yellow element a fully isotropic element. From these figures several observations can be made. First and foremost is that the highest degree of anisotropy is measured along the left and right edge

of the tissue. There is also a high degree of anisotropy left and right of the soft inclusion. Above and below the soft inclusion however, the tissue is more isotropic. Secondly the fibres follow a pattern, where they will generally align in the loading direction, and follow the edges of of the geometry both at the soft inclusion and the left and right edge of the geometry. Both these observations are shown most clear in the top right quarter of the tissue, even though they generally apply to all four quarters of the cultured sample.

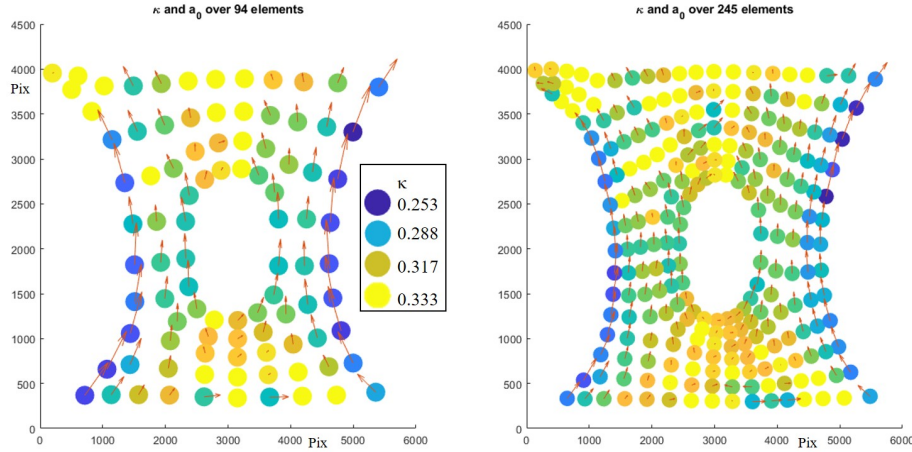


Figure 15: Fibre dispersion and orientation based on three depths at two mesh densities, left at 94 elements, right at 245 elements. The direction of the arrow displays the peak fibre angle, the size of the arrow and the colours of the circles depict κ per element.

3.1.3 Mapping local material parameters to FE models

To implement the local fibre orientation based on the results in Figure 15 in the ABAQUS simulations, the elements were grouped together. The six element groups, based on similar fibre organisation, are shown in Figure 16. The κ values per element subgroup are given in Table 3. The peak fibre angles of each element in group 1 and 2 is equal to the angle of the outer edge of the element. In group 3, the peak fibre angle of each element is parallel to the angle of inner edge of the elements, so the nodes which make up the border with the soft inclusion. For group 4 and 5, the fibers follow the loading direction. Group 6 is deemed fully isotropic and thus has no peak fibre angle.

As can be seen in Table 3 the differences in the average fibre dispersion per element subgroup between the two mesh densities are relatively small. The eventual κ per subgroup used in the simulations is the average of the two measured κ values. As shown in Figure 16, is the only difference between the geometry of the groups between the two mesh sizes in group 5, which is wider in the 245 element versions, though the difference in κ and a_0 between the two mesh sizes in that region which differs is small.

Table 3: κ per group for 94 and 245 elements

Group	94 elements	245 elements	Simulations
1	0.2631	0.2639	0.263
2	0.2979	0.2993	0.298
3	0.2993	0.2978	0.298
4	0.3067	0.3054	0.306
5	0.3206	0.3010	0.317
6	0.3330	0.3309	0.333

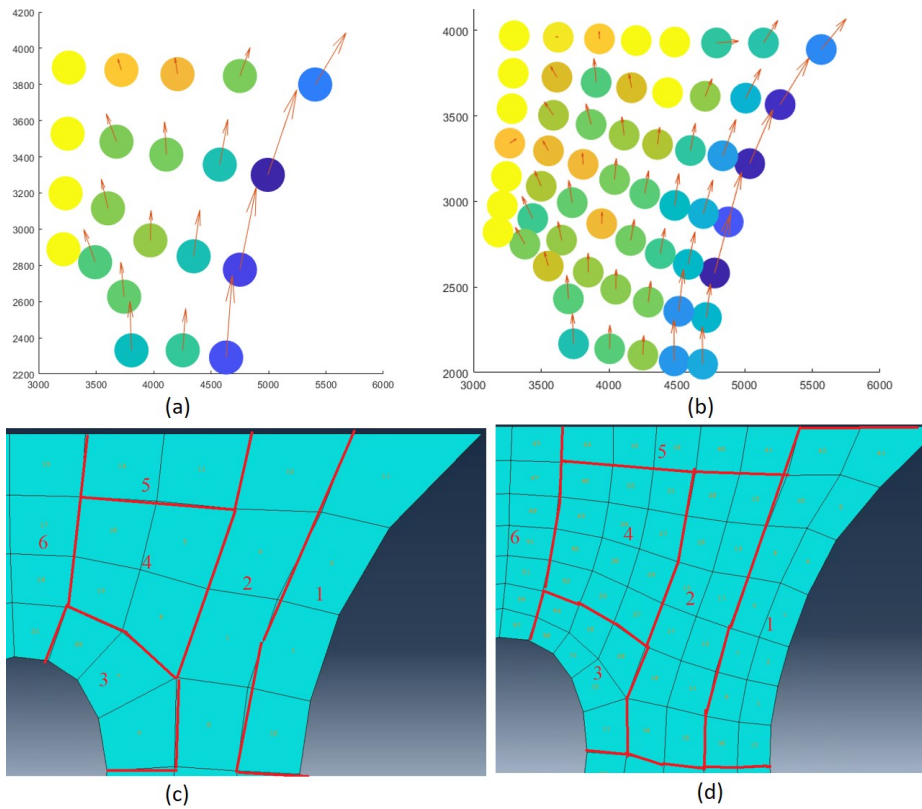


Figure 16: (a) κ and a_0 at 94 elements for top right quarter, based on the stained sample. (b) κ and a_0 at 245 elements for top right quarter. (c) Elements which are combined into 6 subgroups, based on similar k and a_0 values from (a). (d) Element groups based on (b).

3.1.4 Effects local material parameters on stress-strain curve

To measure the effects of the κ and a_0 on the stress-strain curve with the set global parameters, two sets of tests were done on a single element in ABAQUS. On one set the a_0 varied at increments of 30 degrees at a fixed κ at 0.27. At zero degrees, the peak fibre angle is perpendicular to the stretch direction. At 90 degrees the peak fibre angle is parallel to the displacement. The κ had to be lower than $\frac{1}{3}$ to make the material anisotropic. To properly visualize the

difference between the angle sets, one of the lower values of κ found in any element from the stained sample was chosen, leading to a κ of 0.27.

As can be seen in Figure 17, the relative angle of the peak fibre angle to the load has a major impact on the stress-strain curve, where at 30 percent strain, the fully aligned peak fibre angle (purple) has a stress 48 times higher than the perpendicular peak fibre angle. This result also shows that the collagen fibers in this model, with the used material parameters, are indeed the primary load-bearing structure, as is suggested by Akyildiz [6].

In the other set of simulations, the peak fibre angle is set at 90 degrees, parallel to the load, and the fibre dispersion κ is varied over the range found in any element in the tilescan. From the results shown in Figure 17, it is concluded that the κ also has a major effect on the stress-strain curve of the material, as the stress at 30 percent strain at $\kappa = 0.24$ is eight times the stress for the isotropic material properties at similar strains.

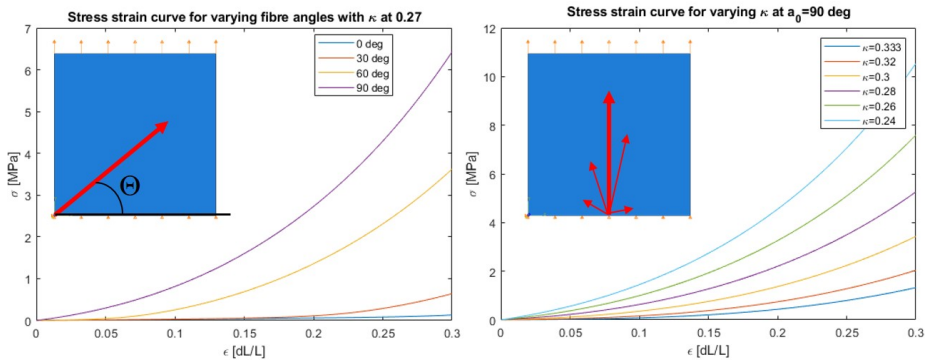


Figure 17: Stress-strain curves of a uniaxial tensile test of a single element with varying a_0 (left) at a fixed κ of 0.27 and a stress-strain curve with varying κ at a fixed a_0 parallel to the loading direction (right). The material parameters C_1, k_1 and k_2 are based on Table 2.

3.2 FEM of uniaxial tensile tests of tissue engineered samples

The results of the simulated uniaxial tensile test of sample 1 are shown in Figure 18, where the max principal stress and strain at the increment before XFEM, and thus rupture, initiates is visualized for the isotropic and anisotropic simulations. In the isotropic simulation, stress is highest left and right of the soft inclusion with a peak max principal stress of 1.9 MPa. In the anisotropic simulation stress is still high left and right of the soft inclusion, but the highest stresses occur on the left and right edge of the geometry with a peak max principal stress at 6.8 MPa. For both the simulations featuring isotropic and anisotropic material parameters, there is a general distribution of higher stresses and strains in the midsection of the sample, at the height of the soft inclusion, and lower stresses and strains above and below the soft inclusions.

The strains in the isotropic simulation are somewhat similar to the stress in its distribution, with the largest strains found at the height of the soft inclusion. The strains however are higher at the edges of both the geometry and the

soft inclusion, where the stress is more evenly distributed. In the anisotropic simulation, the strain is even more localised in comparison with the strains in the isotropic simulation, with a peak strain of 29.98 and 29.32 percent respectively at the top right edge of the soft inclusion. Finally it can be observed that some elements of the anisotropic simulation in the top left of the geometry show large strains.

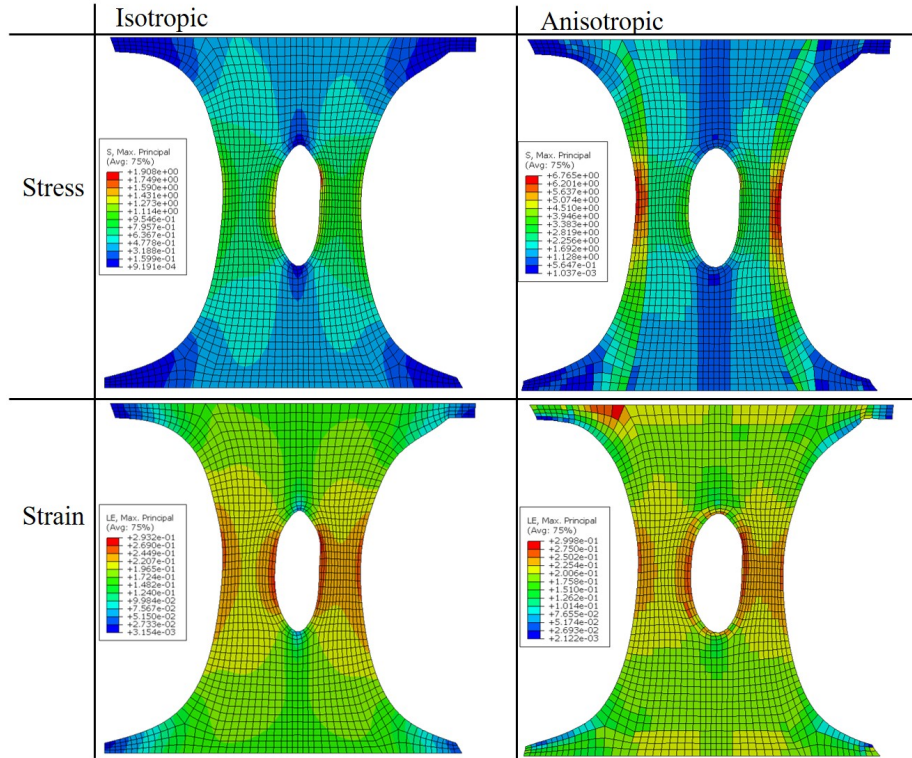


Figure 18: Max principal stress (top) and strain (bottom) results for sample 1 for the isotropic (left) and anisotropic (right) material properties.

To show the strain and stress evolution during the uniaxial test, the average stresses and strains were calculated in four regions; the two sides of the soft inclusion (SI) and the two edges of the tissue near the SI, as shown in the illustration in Figure 19. The curve displaying the relationship between the max principal stress and the y displacement of the top of the sample shows that there is negligible difference in average max principal stress between the edge and the SI in the isotropic sample. The anisotropic simulation however shows much higher average max principal stresses, with the edge undergoing the highest average max principal stress. The differences in strain however are much smaller between both isotropic or anisotropic, and between the two regions, where the highest strains are found on the left and right edge of the SI in the anisotropic sample.

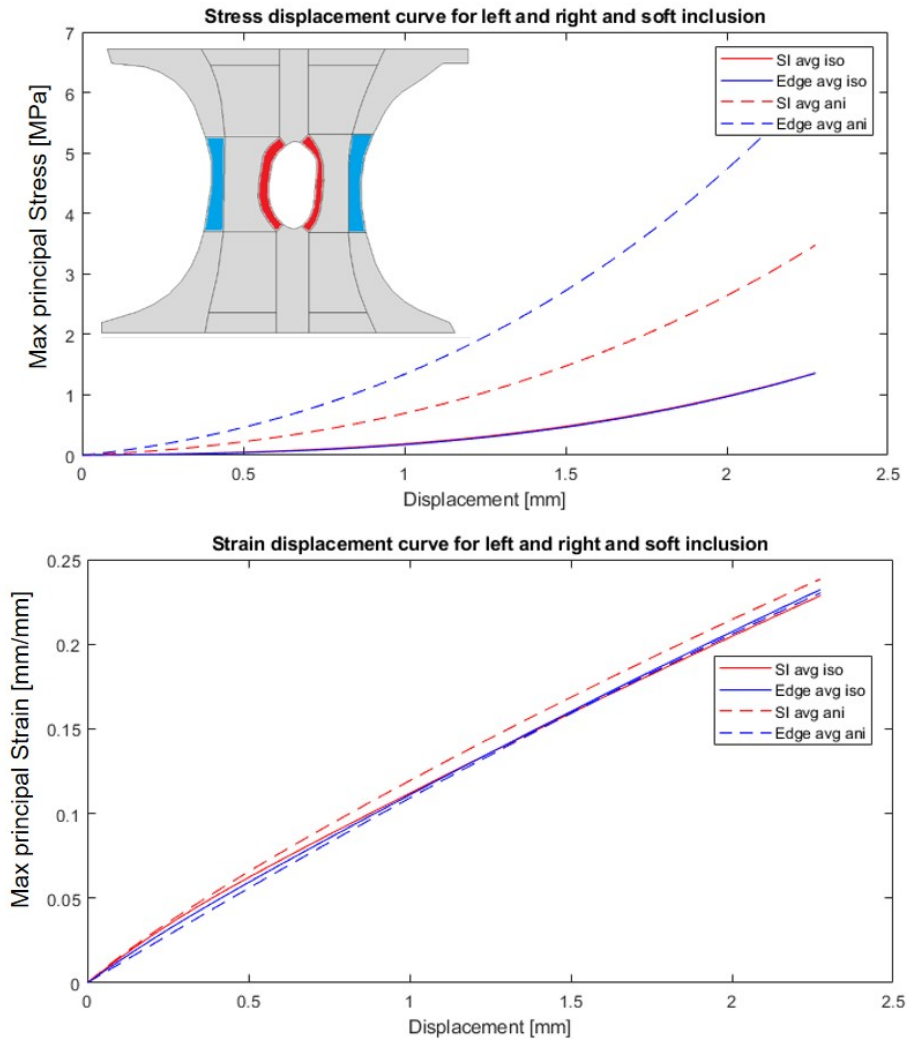


Figure 19: Average max principal stress (top) and max principal strain (bottom) displacement curves of sample 1 for the elements in the edges of the soft inclusion (red) and edges of the geometry (blue).

The max principal stresses and strain distributions at the last increment before rupture initiates of all four samples are shown in Figure 20. The highest measured max principal stress and strain per simulation are found in Table 4. The observations done regarding sample 1 are generally applicable to all four samples. In the isotropic versions, the peak max principal stresses occur at the height of the SI over the entire width of the sample, as do the max principal strains. In the anisotropic simulations, the stresses are highest in the edges of the geometry. The max principal strains are also more localized near the SI in the anisotropic simulation in comparison with the isotropic ones. In the anisotropic version of sample 3, besides the stress peak on the edges, there is also a lower max principal stress peak near the soft inclusion.

In sample 4 it can be noticed that the highest max principal strains are at

the lower right bottom of the SI, rather than at the sides. The highest measured max principal stresses are between a factor 3 and 4 higher in the anisotropic simulations. The highest measured max principal strains differ marginally between the two simulations per sample, except for sample 2 and 4, where the anisotropic strains are 3 to 4 percent higher.

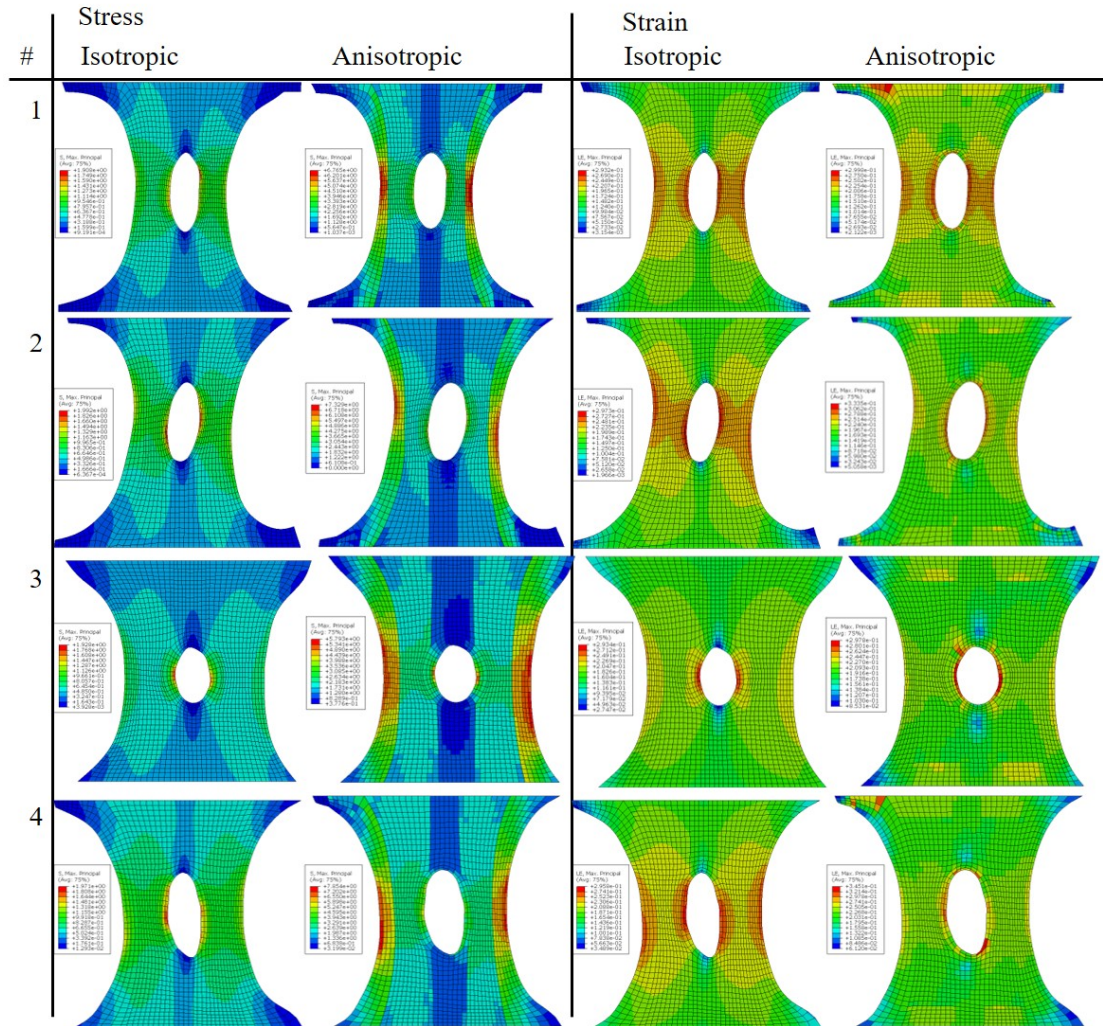


Figure 20: Max principal stress and strain distributions at the increment before damage initiation for 4 simulated isotropic and anisotropic samples.

Table 4: Highest max principal stresses and strains in isotropic and anisotropic versions of the four simulated samples.

Sample	Isotropic Stress [MPa]	Anisotropic Stress [MPa]	Isotropic Strain [dmm/mm]	Anisotropic Strain [dmm/mm]
1	1.91	6.77	0.293	0.300
2	2.00	7.33	0.297	0.334
3	1.93	5.79	0.293	0.298
4	1.97	7.85	0.296	0.345

The test regarding two different mesh densities, and the effect this had on the stress and strain during the hyperelastic part of the simulation is visualized in Figure 21, at a displacement of 1.48 mm and 0.46 seconds. The highest max principal stress found in both simulations are 0.924 MPa and 1.04 MPa for the low and high mesh densities respectively. The location of this peak stress and the overall distribution of stress are similar for both simulations. The max principal strain at this displacement is 23.4 and 24.3 percent for the low and high mesh density sample. The location of the highest strain and the overall distribution of strain are similar for both simulations.

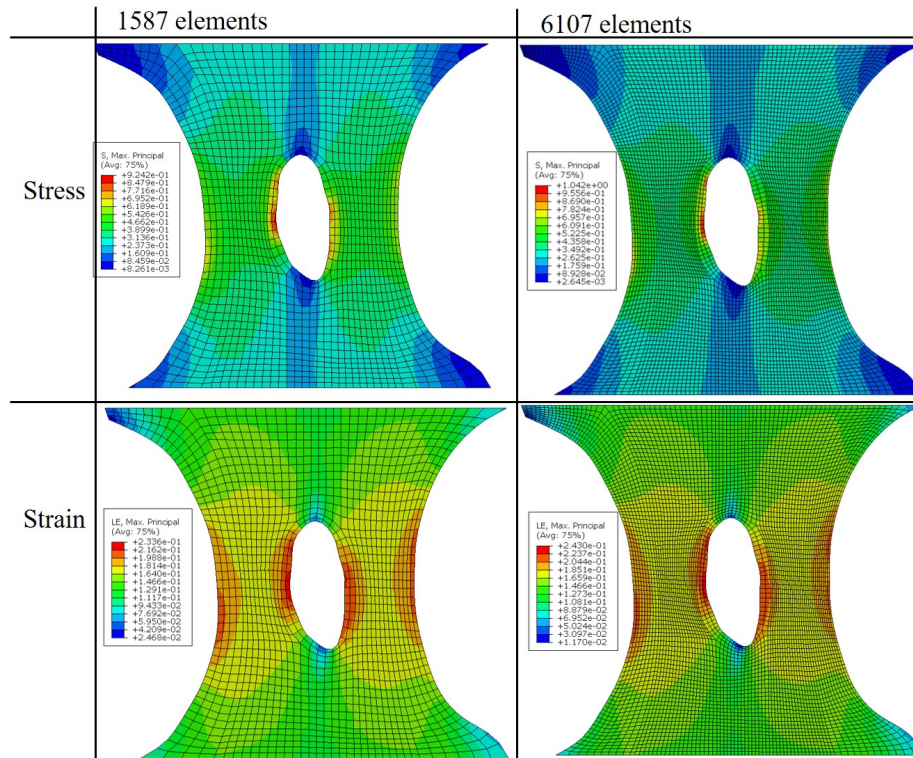


Figure 21: Max principal stress (top) and strain (bottom) results for isotropic sample 4 for the low mesh density (left) and high mesh density (right) at similar displacements.

3.3 Modeling tissue rupture using XFEM

To qualitatively compare the rupture behaviour in the ABAQUS simulations with the rupture behaviour of the cultured samples, the location of the rupture initiation location is compared in Figure 22. Since the rupture for all cultured and simulated samples occurs near the SI, the images and simulation results are zoomed in on this location. The rupture initiation locations are marked with red and green arrows. The location where the first rupture initiates is marked with red, and any ruptures occurring later in the simulation are marked in green. Two initiations starting simultaneously are marked in with a similar colour. The images of the simulations show the maximum principal strain distribution.

Figure 22 shows that the damage initiation location within the SI is similar between the isotropic and anisotropic simulations for all samples. The order in which damage initiates (left vs right edge) is also similar for all four samples between the two versions of the simulation. Isotropic sample 2, 3 and 4 do however have extra damage initiation locations on the sides of the tissues, where the anisotropic simulations do not.

The damage initiation locations of the simulated samples differ from the damage initiation locations of the cultured samples in several ways. For sample 1, the locations of rupture initiation in the simulated samples differ from the cultured sample, as does the order of rupture between left and right edge of the SI. For sample 2 both simulations accurately represent the location and order of damage initiation in comparison with the cultured sample. Though in the isotropic simulation, there is an extra damage initiation location on the left side of the sample. Though for sample 3 the location of rupture initiation in the simulated samples inside the SI is similar to the ones in the cultured sample, the order is not, as in the cultured sample there is a clear primary and secondary rupture, where in the simulations the damage initiates both left and right of the SI simultaneously. Furthermore, in the isotropic simulation of sample 3 two damage ruptures initiate later in the simulation at the sides of the sample. The location of damage initiation of the simulations of sample 4 are somewhat similar to the cultured sample, the order however is not, as the right side of the SI ruptures earlier in the cultured sample. Finally, an extra damage initiation location occurs on the left side of the isotropic simulated sample.

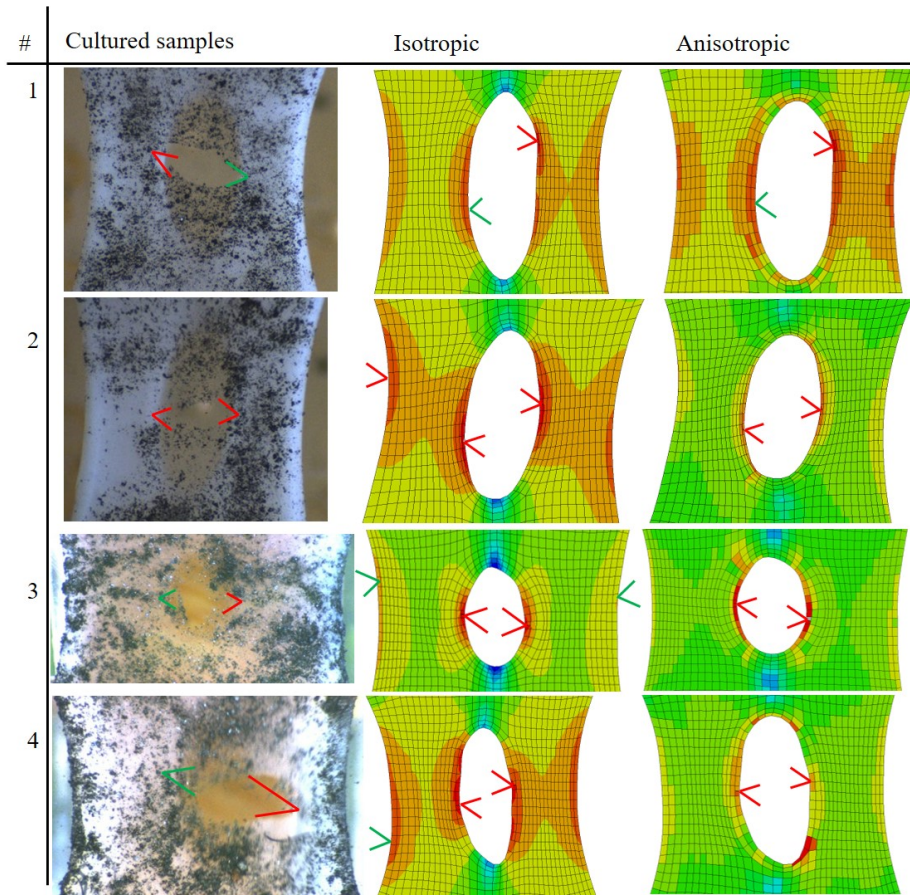


Figure 22: Rupture initiation locations based on the images of the four cultured samples (left), the isotropic ABAQUS simulations (middle) and anisotropic simulations (right). The location of the first rupture initiation is marked in red, a second initiation in green. If two initiations start simultaneously, both are marked red. The two columns visualizing the simulations display the maximum principal strain.

There is a large disparity between the four cultured samples regarding the rupture propagation. For cultured sample 1, during the experiment the rupture propagates through the entire tissue after one and before the next image, as the video was converted to images with a sampling rate of 15 HZ. Therefore no rupture propagation path can be determined other than that the entire sample ruptured within 70 msec. The images of cultured sample 2 during the uniaxial tensile test show no sign of damage, until full rupture occurs within 200 msec. Sample 3 slowly ruptures over several seconds, showing a clear rupture path. Sample 4 quickly ruptures on the right edge, after which the left edge takes 1.2 seconds to fully rupture. The rupture behaviour of the cultured samples over time can, besides using the available images, be determined based on the force displacement curves, shown in the left graph in Figure 23.

This rupture behaviour over time for the isotropic and anisotropic version of the four simulated samples is visualized in the right graph in Figure 23.

Here the reaction force at the bottom of the samples is measured over the y displacement of the top of the sample. Both the force displacement curves from the experimental results and computational results show a hyperelastic curve, which have a distinctive toe region, elastic region and damage region. All four anisotropic samples show a factor two to three higher reaction force in comparison with their isotropic counterparts. The displacement at which damage initiates is slightly higher in samples 1, 2 and 3 with isotropic material parameters compared to the anisotropic simulations.

Cultured sample 3 and 4 show similar elastic force displacement curves as cultured sample 1 and 2. The force displacement curves of simulated sample 3 and 4 however have a much steeper force displacement curve for both the isotropic and anisotropic versions in comparison with sample 1 and 2.

The displacement at which damage initiates according to the force displacement curves of the simulations approximates the damage initiation of the cultured samples 1 and 2. In sample 3 the simulation appears to start rupture at a higher displacement, and in sample 4 the damage initiates too early in the simulations.

The force displacement curves of the cultured samples have a different scale of reaction force in comparison with the anisotropic samples, with the cultured samples giving around 2 N of maximum reaction force, where the anisotropic simulations give a maximum of around 12 N. Finally, the full rupture in the cultured samples can be seen by the decrease of force to 0 N. Even though the simulations do show decreases in reaction forces, this never reaches 0 N. Most force displacement curves of the simulated samples show a generally similar rupture propagation over time. Isotropic sample 1, 2, 3 and anisotropic sample 3 and 4 show a sudden and sharp decrease in reaction force when rupture starts. In isotropic sample 4 and anisotropic sample 1 and 2 there are several peaks in the force displacement curves.

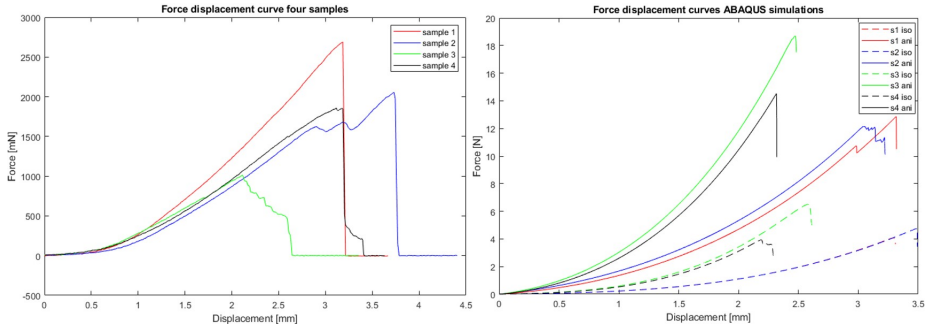


Figure 23: Force displacement curves for the four cultured samples (left) and their respective isotropic and anisotropic simulations (right). The dashed lines regard the isotropic simulations, the solid lines the anisotropic simulations. Note that isotropic sample 1 highly overlaps with isotropic sample 2.

All four cultured samples rupture horizontally from the SI up to the start of the edge section. When the edge section is reached, the rupture propagates vertically, so parallel to the collagen fibers, until the tissues completely rupture following a horizontal rupture path again. In sample 1 this can only be based on the geometry of the ruptured results. The damage in the simulations always

propagates horizontally, as shown in Figure 24. All simulated samples only show rupture propagation paths starting from the SI, except for the isotropic simulation of sample 4 and to a lesser degree isotropic sample 2 and 3. Here an additional rupture propagates starting from the left edge of the geometry. Though in the isotropic simulation of sample 1 ruptures initiated in the edge of the geometry, this did not propagate. Only the isotropic simulation of sample 2 completely ruptures on both sides of the SI. In isotropic sample 1, 3 and 4 and anisotropic sample 1 and 4 completely rupture on 1 side of the SI. After these ruptures the simulation diverges. The simulations of anisotropic sample 2 and 3 diverge before one rupture propagates through the entire sample.

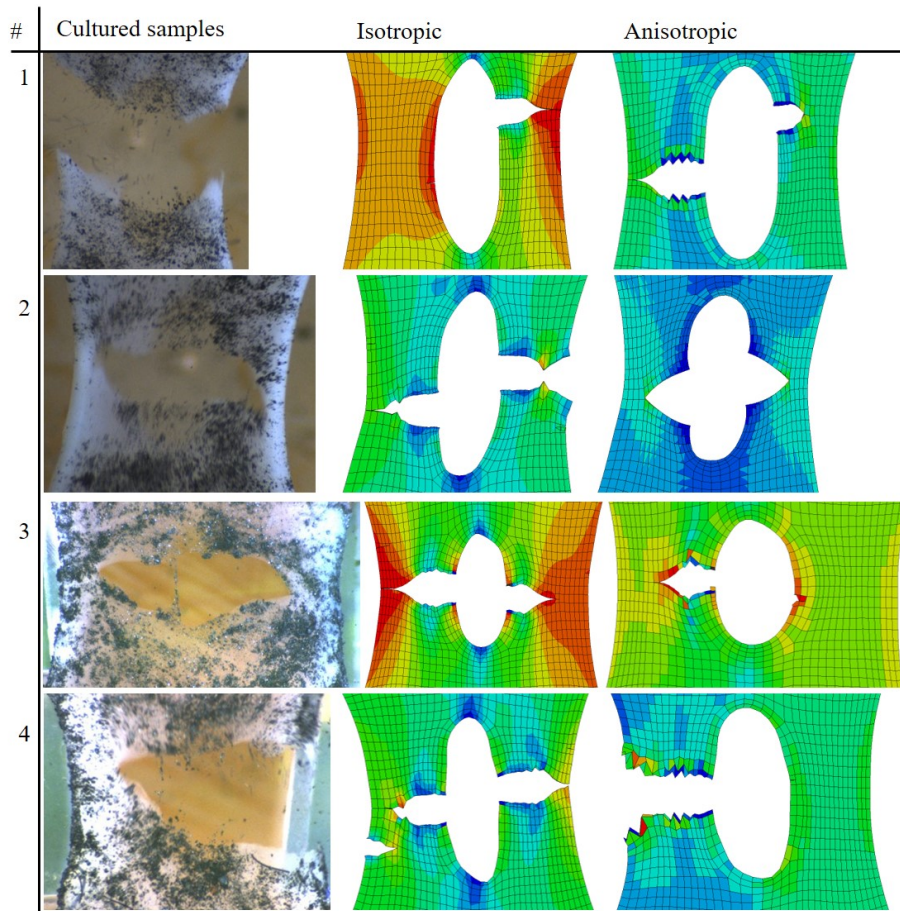


Figure 24: Rupture propagation paths visualized for the four cultured samples (left), the isotropic ABAQUS simulations (middle) and anisotropic simulations (right). The simulations visualize the max principal strains.

4 Discussion

4.1 Material parameters

4.1.1 Material model

The HGO model is a widely used material model to simulate soft biological tissues and is a material model available in ABAQUS. Combining the HGO material model for the elastic response with XFEM for the damage response however does not allow for separate damage properties for the EMC and the collagen fibers. Gültekin suggests that these two parts of the material should be considered with two distinct failure processes.[17] Rather than base the damage initiation on a fixed strain or stress, as is the case when using XFEM, the damage can also be based on the strain energy within the system. This would allow for a separate damage factor for both the EMC and the fibers, as done by Natali[18] and Calvo [19]. These damage factors alter the amount of strain energy an element can hold by a damage factor based on previously encountered strain energy. This decrease in allowed strain energy decreases the stiffness matrix. This damage criterion can be implemented in ABAQUS using a user subroutine UMAT. A UMAT can be used to define the mechanical constitutive behavior of a material. Over the course of several months an unsuccessful attempt was made to implement this damage model in ABAQUS. Based on the UMAT, once an element starts to endure Damage, the stiffness decreases. This leads however to larger strains, which leads to more damage. This positive feedback loop lead to immediate divergence issues within ABAQUS. Therefore the decision was made to use XFEM to replicate the damage behaviour of the cultured samples.

4.1.2 Global material parameters

Figure 12 shows that the force-displacement curve of the simulated sample accurately replicates the experimental results of the cultured sample at lower displacements, but becomes steeper at higher displacements. The choice to focus on accurately representing the lower displacements of the experimental curve was deliberate, as at higher displacements micro damage starts occurring in the cultured sample (blue), but no damage occurs in the simulation results (red). Therefore the simulation should show a steeper slope at higher displacements. At what displacement micro damage initiates however can't be accurately determined based on the available images of the experimental results. Therefore the derivative of the force displacement curve of the experimental results was regarded, which shows a drop at a displacement of around 2.3 mm, as can be seen in Figure 25.

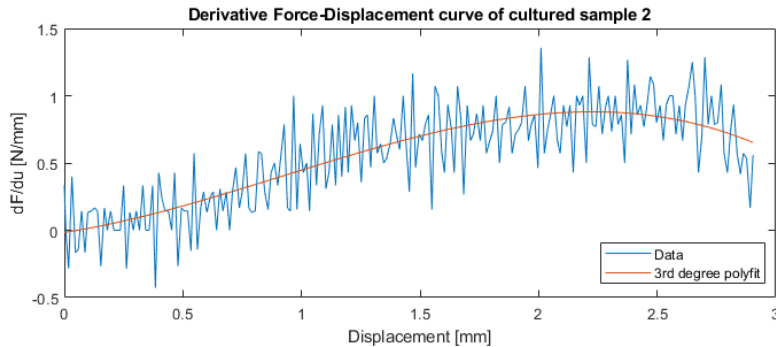


Figure 25: Derivative of the force displacement curves from the experimental results from the uniaxial tensile test of sample 2. The derivative starts to decrease at around 2.3 mm.

It can be noticed in Table 2 that the value for k_1 is significantly higher than C_1 . This shows that the fibrous part of the strain energy equation is dominant over the EMC part, which shows that the collagen network is the main load bearer, which is in agreement with literature[6].

A limitation of the determination of the global material parameters is that the material was assumed to be homogeneous and isotropic. Based on the determined fibre organisation of the stained sample, it is clear that the tissue is anisotropic, where the degree of anisotropy depends on the location within the sample. The local material parameters k_1 , k_2 and C_1 could not be determined based on the data available from the stained sample, therefore no conclusion could be drawn regarding the homogeneity of these material parameters of the cultured samples.

Another limitation of the study is that all four simulated samples were based on the global material parameters of sample 2. Based on the comparable force-displacement curves of the four tested samples shown in Figure 23, and the similar geometries of the four cultured samples, it can be concluded that their elastic global material properties are in the same order of magnitude. For this study an approximation of the global material properties is sufficient, as slight differences in material properties will not majorly affect the location of rupture initiation and propagation. This is due to the fact that strain mostly depends on geometry, and less so on the material properties. Furthermore, the results regarding the damage initiation and propagation are based on the comparison between the isotropic and anisotropic simulations, which have the same input of global material parameters.

A third limitation of the used methodology regarding the determination of the global material parameters is added by the geometry of the cultured model. The simulation used to calculate the material parameters was a 3D sample which assumed a uniform thickness of 0.6 mm, where the actual sample thickness varied between 0.54 and 0.76 mm. This difference in thickness most likely leads to a different force-displacement curve in the uniaxial tensile test results, and therefore leads to a margin of error in the determined global material parameters.

Finally it was noticed during the different manual iterations, that k_2 had a relatively small impact on the force displacement curve. Increasing the k_2

value from 2.5 to 13 only lead to a 1.5 percent increase in reaction force at a displacement of 2.45 mm. Therefore there is a large margin of error in the determination of the k_2 value.

4.1.3 Local material parameters

When regarding the peak fibre angles at the different depths in Figure 13, It must be noted that the fibre dispersion is not taken into account in these results. So a κ of $\frac{1}{3}$, which represents total isotropy of the fibers, would still show one peak angle, but in a random direction. The peak fibre angles in Figure 13, and the original images of the stained sample in Figure 8, show that where the image is poorly lit, the peak fibre angles are much less organised. Based on the negligible differences between the 94 and 245 element peak fibre angle distributions, it can be concluded that the mesh and image density has no effect on the results.

A comparison between the peak fibre angle organisation and the fibre dispersion organisation in Figure 13 and 14 shows that the distorted angles are generally in elements with a κ of $\frac{1}{3}$. Therefore these disorganised peak fibre angles do not effect the material model of the simulations, as these elements will have isotropic material behaviour.

Regarding the results of the local fibre organisation, there are two systematic inaccuracies for all six results, shown in Figure 14 due to image quality. The top left corner is poorly lit as can be seen in Figure 8, which leads to FibLab not being able to identify any fibers and thus no fibre angles. This leads to the random directions of the peak fibre angles here. As no angles could be found, the κ was manually set at $\frac{1}{3}$. The distortion of the peak fibre angles in the bottom right corner can be explained by the dried up embedding fluids which are visual in the images of the cultured sample in Figure 8. This is a limitation as it limits the data available as input for the material model.

Based on the observation that for all four quarters of the tissue there is a generally similar distribution in κ and a_0 , the conclusion can be drawn that the tissue is symmetric with respect to the x and y axis, where the origin is in the middle of the soft inclusion. Since the image quality and the data is most in line with the observations in the top right quarter, this quarter was used to draw further conclusions. This does mean that only a quarter of the available data regarding local fibre organisation is used as input for the local material parameters in the FEM simulations.

The most important limitation in finding the local material parameters is the fact that only one stained sample was available. Therefore no calculations can be done regarding the variance of local fibre organisation between samples.

4.1.4 Mapping local material parameters to FE models

Implementing the local fibre orientation and dispersion into the simulations of the four samples was done by grouping the elements into subgroups. The elements were grouped based on the minimization of differences of κ and a_0 values within one element subgroup and how they could be implemented into ABAQUS using Matlab. The eventual decision to make six groups, and the geometries of these groups, was determined manually, rather than based on an optimization scheme.

Though the grouping and averaging of local material parameters will lead to less local errors, it also will lead to round-off errors. How large these round-off errors are regarding the rupture behaviour is unclear, but based on the results shown in Figure 17, it is clear that, with the used global material parameters, even an increase in κ of 0.02 can lead to a 40 percent stress increase at 30 percent strain. Therefore this is a limitation in this study.

Another limitation in this study is the fact that the stained sample did not undergo a uniaxial tensile test. The local fibre organisation of the four samples that did undergo uniaxial tensile test could not be determined. Therefore the assumption had to be made that the local fibre organisation of all five samples was equal.

The six element subgroups, shown in Figure 16, were replaced by five groups. Groups 2 and 4 were combined to achieve a mesh which allowed for less divergence problems in the simulations. This change however has limited effects on the results, as the peak angle per element didn't change due to the new groups.

4.2 FEM of uniaxial tensile tests of tissue engineered samples

The isotropic simulation of sample 1, shown in Figure 18, shows that the stress and strain distribution are highly dependent on the geometry of the sample, as there is significantly higher stresses in the thinner parts of the geometry, left and right of the soft inclusion.

From the anisotropic simulation it can be concluded that the stress values and distribution are also highly affected by the local material properties as they differ greatly from the isotropic simulation. The outer edges on the left and right edge of the geometry endure high strains due to the geometry. This combined with the high stiffness in these regions due to the low κ and a_0 in the direction of the strains leads to high stresses in these regions. Though the strains are largest in the left and right edge of the soft inclusion, the lower stiffness in these regions leads to lower stresses.

There are a few elements in the anisotropic sample with high strains on the top and bottom edge where these do not occur in the isotropic version. These are due to stresses in the material which are to a varying degree perpendicular to the fibre orientation. This leads to higher strains as there is little stiffness in the direction perpendicular to the fibres, as discussed in Chapter 3.1.4.

The max principal strains averaged per group, shown in Figure 19, show that there are small but noticeable differences between the isotropic and anisotropic results. There is a high strain on the left and right edge, at the height of the soft inclusion. The edges of the soft inclusion show the highest strains within the sample. From these two figures it can be concluded that in this sample, the geometry of the sample is a much bigger factor than local material properties on where large strains occur. However, the anisotropic local material parameters do increase the difference of highest strain between the edge of the SI and the geometry edges. These observations described for sample one apply to all four samples, where the max principal strains are heavily dependent on the geometry, and somewhat on local material properties, and the max principal stresses are dependent on both geometry and local material properties.

Regarding the mesh density results, the difference in max principal stresses and strains between the low and high mesh densities of around 10 and 4 percent

difference respectively is rather high. The stress and strain distribution are however more important for this study than the actual peak stresses and strains at a certain increment, as the distribution leads the determination of the damage initiation location. Since the differences in distribution of both max principal stress and strain between the two mesh densities are negligible, and XFEM calculations are computationally expensive, the decision was made to use around 1500 elements per simulation.

There are several limitations in the presented methods regarding the hyper elastic uniaxial testing. First there is a margin of error in the geometries in comparison with the actual geometries of the cultured samples. This is due to the soft inclusion having a thin top layer, which makes the distinction between the soft inclusion and the actual tissue hard to see based on the available images.

Secondly the tilescan, shown in Figure 7, consists of 90 to 99 percent anisotropic tissue according to the local fibre orientation discussed in the research. The remaining one to ten percent is the top section, which is nearest to the camera, is anisotropic as well, but with all fibers aligned in the loading direction [9]. By how much this top layer might have increased the calculated κ values is unclear. The camera was however able to take pictures at several depths in the stained sample, which should minimize the effect of the top layer.

4.3 Modeling tissue rupture using XFEM

Based on the damage initiation locations in both the simulations with isotropic and anisotropic material parameters, it can be concluded that the damage initiation locations are dependent on the geometry, as well as on the local material parameters. As expected do both the cultured samples and all simulations rupture left and right of the soft inclusion, where the cross section surface is smallest. The local material properties also have an effect on the damage initiation locations. Due to the higher stiffness of the elements in the sides of the geometry by applying the local fibre organisations, the strains are lower there in comparison with the elements in the isotropic simulations. As the damage initiation threshold is based on maximum principal strain, these lower strains lead to the elements in the anisotropic simulations not to rupture, where they do in the isotropic simulated samples.

When regarding rupture initiation location of the anisotropic simulation of sample 2 and 4 in Figure 22, the maximum principle strains of the elastic simulations in Table 4, and the set max principle strains for damage initiation in Table 1, the maximum principle strains measured before rupture initiates are higher than the strain threshold. In sample 4, the highest max principal strains occur on the bottom right of the soft inclusion, rather than at the rupture initiation location. The strains are high here due to the fibres having a more horizontal peak fibre angle, but the induced stresses are vertical. The elements here do not rupture however due to these elements being outside the enriched regions. Only the sides of the SI are enriched regions, as this was where damage should occur based on the cultured samples. This is a limitation of this study, as it forced the damage to occur at the sides of the SI.

Regarding the force displacement curves of the simulated samples in Figure 23, the higher force displacement curves of the anisotropic simulations are due to the higher stiffnesses in the edges of the geometries.

The higher damage initiation displacement of isotropic samples 1, 2 and 3 in

comparison with the damage initiation of their anisotropic counterparts is due to the more localised highest strains near the SI in the anisotropic simulations, as shown in Figure 19. In sample 4 the anisotropic simulation ruptures at a higher displacement. It is hypothesised that this is due to the non-rupturing elements at the bottom of the SI. As these elements are less stiff than the rupturing elements, they take some of the strains away from the rupturing elements, allowing them to rupture at a higher displacement.

The higher force-displacement curves of the simulations of sample 3 and 4 in comparison with sample 1 and 2 are hypothesized to be due to the geometry, as sample 3 and 4 have a lower length to width ratio in comparison with the other samples (1.9 1.7 1.2 and 1.4 for the four samples). Since the global material parameters are equal for all four simulated samples, this will lead to a steeper force-displacement curve. The force displacement curve of cultured sample 3 and 4 however is very similar to cultured sample 1 and 2. Based on these observations it is hypothesized that the cultured tissue of sample 3 and 4 is therefore less stiff than cultured samples 1 and 2. As all four samples have a generally similar average thickness of 0.54 mm, these effects should be minimal.

The damage initiation of the simulated samples could be altered by setting a different damage initiation strain threshold. This allowed for similar damage initiation displacements of samples 1 and 2. The damage initiation of simulated samples 3 and 4 differ from the cultured samples according to their force displacement curves. In sample 3 the damage does initiate at the displacements similar to the cultured samples. The force displacement curve however keeps increasing after rupture initiates. This is most likely due to the high set Fracture energy. In sample 4, the damage initiation is at too low a displacement. This is due to the high strains occurring in sample 4. A 38 percent strain threshold is necessary to accurately reproduce the damage initiation displacement. The simulations however diverge immediately after rupture initiation above a damage initiation strain threshold of 30 percent.

The scale of force differences between the cultured samples and the anisotropic simulations is due to the different stiffnesses of the elements in the anisotropic samples. As the global material parameters were based on isotropic sample 2, this will lead to the anisotropic simulations being too stiff. Isotropic samples 1 and 2 do have similar elastic force-displacement curves in comparison with the cultured samples.

The rupture propagation paths of anisotropic sample 1, 2 and 3 are due to the rupture propagation paths hitting element nodes. This can lead to halting the rupture propagation path. As the displacement continues, this leads to a new peak in reaction force before a new rupture occurs or the simulation diverges.

Regarding the rupture propagation speeds of the cultured samples, it is clear that this parameter differs greatly between cultured samples. What biomechanical parameters control these different rupture propagation speeds warrant future research. The rupture propagation speed of the simulations could be somewhat altered by changing the set fracture energy.

The rupture propagation paths of the simulations in Figure 24, show that local material parameters can alter the simulated damage propagation paths. This is evident in isotropic sample 4, and to a lesser degree sample 2 and 3, where an additional rupture propagates from the left edge, which does not occur in the anisotropic simulation. This shows that the anisotropic simulations more

accurately represent the rupture of the cultured samples. In anisotropic sample 1, the rupture propagates first at the right side of the SI, similar to the isotropic simulation. Only after hitting a node does the left side of the SI propagate. For sample 2 and 3 the rupture propagation paths are similar, apart from the point at which the simulation hits a node, and diverges. In anisotropic sample 4 the damage does not propagate due to the lower strains at the right side of the SI, due to the large strains in the elements on the bottom right of the SI. Finally it must be stated that the anisotropic simulations do encounter more divergence issues, with two out of four simulations diverging before a rupture fully propagates through one half of the tissue.

4.3.1 Lessons learned regarding XFEM

The goal of the application of XFEM in this research was to replicate the damage initiation and propagation of the cultured samples in an ABAQUS simulation. The lessons learned regarding implementing XFEM in the performed simulations are described in this subsection.

The mesh size differences within one simulation can have a major impact effect on the measured stresses and strains of different elements. Even though there is minor effect on the results if all elements are equally smaller, as seen in subsection 3.2, mesh density does become an important factor when the difference in element size is too large within one sample. Making sure the mesh size is roughly similar took some iterations due to the many partitions within the sample required for the different material groups, as shown in Figure 16.

Another consideration regarding the meshing of the samples is the crack propagation path. In Figure 24, it can be seen that the crack propagation path hits a node anisotropic sample 1, 2 and 3. Once the crack path hits a node, this could lead to a halt in the damage propagation. To minimize the chance of the crack path hitting a node, the mesh was manipulated using partitions to have an almost rectangular mesh left and right of the soft inclusion, to ensure a horizontal crack path through the middle of all elements could be achieved. The groups determined in Figure 16 are therefore different than the eventual groups used in the simulation which are shown in Figure 19.

At what point the ABAQUS simulation diverges and thus quits when performing the XFEM part of the simulation highly depends on values chosen for the parameters shown in Table 1. Both the Damage evolution energy parameter and the viscosity coefficient were iteratively determined to ensure a maximum propagation. The trade off with using the viscosity coefficient however is that the higher the coefficient value, the higher the difference in Strain energy due to viscous dissipation. This difference can be calculated by determining the ratio between the total strain energy of the model and the viscous dissipation in the model. This ratio quickly increases as the propagation continues. Once full rupture occurs the viscous dissipation energy is almost as large as the strain energy in the system itself.

4.4 Recommendations

To compare the elastic results in this article with the real samples, one could perform a comparison study between the elastic strain results from the ABAQUS

simulations and a Digital Image Correlation (DIC) analysis of the cultured samples. A DIC analysis can be used to measure the local strains of the cultured samples. Replicating the local strains of the cultured samples in ABAQUS simulations could lead to finding local material properties which were deemed global in this study, such as the collagen fibre stiffness k_1 . Comparing the location of the maximum local strains in the cultured samples using DIC with the damage initiation locations of the cultured samples could also determine whether maximum strains are a good indicator for damage initiation in these samples.

Based on the results from the stained sample on the local fibre orientation and dispersion, and the local stresses and strains in the ABAQUS simulations, it is clear that there is a lower κ on locations where stresses are higher in one principal direction. Furthermore, the peak fibre angle seem to generally follow the direction of the highest principal stress. If more stained samples were available, a study could be done on the relationship between the stresses occurring in the sample during culturing, and the fibre organisation this culturing will lead to in these tissue-engineered tissues. Literature agrees that fibers will generally migrate and rotate towards best handling applied load[20]. Should this relationship between fibre organisation and endured stresses be proven correct, it could potentially allow for the determination of local material properties based on the geometry of an atherosclerotic plaque alone. This would lead to a workflow where the geometry would be determined by imaging. This geometry would be made into a FE model with isotropic material properties. Based on the locations of higher stresses when applying forces during the simulation, local material properties could be altered to counter the endured stresses, leading to an anisotropic and heterogenous material model. It would be recommended to make the peak fibre angle a_0 dependent on the direction of the largest principal stress. The κ should depend on the ratios and sizes of the two primary stress directions and the shear stress. The higher the stress ratio in one direction, the lower the κ . Another option would be to implement two fibre families for every element, and base the fibre stiffness parameter k_1 or κ on the amount of stress encountered in the fibers principal direction. This potential workflow does however not take into account that collagen synthesis is inhibited in inflamed tissue, which atherosclerotic tissue often is [3].

Based on the results from Chapter 3.2, it was determined that the XFEM damage initiation threshold should be set at a maximum strain, rather than a maximum stress value, since setting a maximum stress value would lead to a damage initiation at the edges, rather than at the soft inclusions. In literature, besides a stress or strain based threshold, often the Strain Energy is used as an indication for an element to initiate the rupture[19][18]. From measuring the Strain Energy per element of anisotropic sample 1, which is visualized in Figure 26, it is clear that the highest Strain energies are at the sides of the tissues. Therefore a strain energy based damage initiation criterion would, in these samples using local material parameters, lead to the simulated samples rupturing at the sides of the geometry, rather than at the SI.

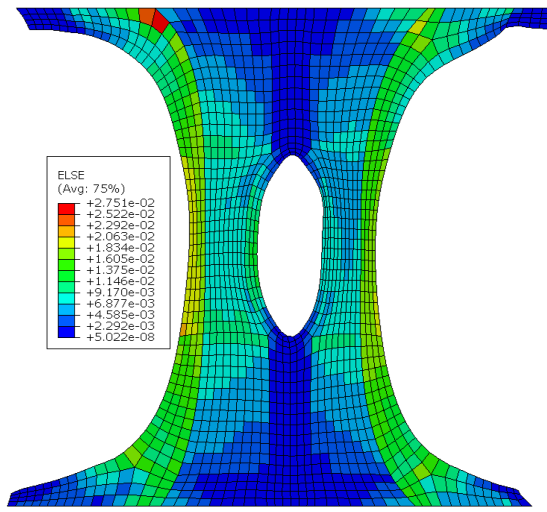


Figure 26: Strain energy per element for the anisotropic version of sample 1.

To comply with the anisotropic stiffness of the samples, one could use a different damage model, for example the Tsai-Wu failure criterion [21], which takes the anisotropy of a material into account when calculating whether a threshold stress has been reached. It does however not take into account different stiffness values within one sample, such as due to changing κ or k_1 values. As the strains in the samples regarded in this research are much more dependent on geometry rather than material parameters, it is recommended to perform a similar rupture study on geometries which more accurately represent atherosclerotic plaque tissue.

5 Conclusion

This study aims to contribute to the making of a numerical model which accurately represents atherosclerotic plaque. This is done by comparing the elastic and rupture behaviour of collagenous micro tissues and their respective finite element models in ABAQUS. The material model of these computational models is based on a combination of global and local material parameters, where the local material parameters are based on the local fibre organisation. A framework was developed to measure the local fibre organisation using provided imagery of a nuclear stained tissue engineered sample and implement the results in four tissue engineered samples.

The collagen fibres in the nuclear stained sample are generally aligned in the direction of loading during culturing, and follow the edges of the geometry. The collagen fibres are generally less dispersed left and right of a soft inclusion, where the stresses endured during the culturing of the samples are highest. The collagen fibres are most aligned on the left and right edge of the sample, and most dispersed above and below the soft inclusion.

A uniaxial tensile test was performed on four cultured samples and replicated in ABAQUS with the material parameters implemented using the Holzapfel-Gasser-Ogden model. Two material models were implemented in the simulations, where one version was isotropic and homogeneous throughout the sample. The other version was anisotropic and heterogeneous due to the implemented local fibre organisation.

From the finite element simulations it is observed that the measured stresses are highly dependent on both the geometry and the material model. The simulations where the material model was isotropic show that endured stresses are highly dependent on the geometry, as the stresses were highest left and right of the soft inclusion, where the cross-sectional area is smallest. Comparing these stresses with the anisotropic simulations which do include local fibre organisation shows that the added stiffness in the elements which have low fibre dispersion leads to a factor 3 or 4 increase in endured stresses. The measured strains are mostly dependent on the geometry of the samples, but are affected by the material parameters. The peak strains in the anisotropic simulations were more localised around the soft inclusion, and were lower around the edges of the geometry due to the higher stiffness in these elements.

XFEM was implemented in the ABAQUS simulations to replicate the damage initiation and propagation of the cultured samples. The damage initiation in the XFEM simulations is based on the maximum principal strain. The anisotropic simulations were mostly able to accurately represent the location of the damage initiation in comparison with the cultured samples. Additional damage initiations occurred in the isotropic simulations due to the lower stiffness at the edges of the geometries. This does not agree with the cultured samples, where based on the imagery damage always initiated from the soft inclusion. The damage propagates mostly horizontal in the cultured tissues and completely horizontal in the simulated samples. The damage in all four simulated anisotropic samples propagates from the soft inclusion outward. In one out of four isotropic simulations an additional major rupture propagates from the edge of the sample inward. In two out of four isotropic simulations a minor additional rupture propagates inward.

Based on these findings it is concluded that implementing the local fibre or-

ganisation to the material model can improve the accuracy of the finite element simulations of collagenous soft tissues, which includes atherosclerotic plaque, as the rupture behaviour of the simulations with anisotropic material parameters more accurately represents the rupture behaviour of the engineered fibrous tissues in comparison with simulations with isotropic material parameters. It is recommended to perform a Digital Image Correlation (DIC) analysis to measure the local strains of the cultured samples and compare them with the local strains of simulations with anisotropic and isotropic material parameters.

Appendix A

Appendix A contains the Matlab scripts required to calculate the local fibre organisation of the available stained sample. The main code given first requires the ABAQUS input file for the nodal coordinates and uses three other scripts. The first code is part of the FibLab package[14]. The last two were provided by the Erasmus MC.

Matlab Code

```
1 %% Main code to calculate the local fibre organisation of
  the tilescan.
2 close all
3 clc
4
5 input_filename = 'samp4xfem.s.inp';
6 fid = fopen(input_filename, 'r');
7 input = textscan(fid, '%s', 'delimiter', '\n');
8 input = lower(input{1}); % Using lower() makes the
  input lower-case,
9 fclose(fid); % so that I don't need to
  worry about
10 clear ans % case-sensitivity
11
12 % Find the rows in the .inp where node/element
  definitions start
13 [start_node, start_element, end_element,
  start_elsetPLAQUE, end_elsetPLAQUE, start_materials,
  end_part] = FindInputSections(input_filename);
14
15 % Node Coordinates in XY-coordinates of ABAQUS model
16 node_XY = NodeCoordinates(input_filename, start_node,
  start_element);
17
18 % Read input file text
19 fid = fopen(input_filename, 'r');
20 input = textscan(fid, '%s', 'delimiter', '\n');
21 input = lower(input{1}); % Using lower() makes the
  input lower-case,
22 fclose(fid); % so that I don't need to
  worry about
23 % case-sensitivity
24 start_element = [];
25 end_element = [];
26
27 for ii=1:length(input)
28     var=input{ii};
29     var=strtrim(var);
```

```

30         if strfind(var, '*element')==1 & isempty(
31             start_element) == 1
32             start_element=ii;
33         end
34     end
35 %end
36 fid = fopen(input_filename, 'r');
37 input_afterelements = textscan(fid, '%s', 'Delimiter', '\n',
38     'HeaderLines', start_element);
39 input_afterelements = input_afterelements{1};
40 fclose(fid);
41
42     for jj = 1:length(input_afterelements)
43         var=input_afterelements{jj};
44         var=strtrim(var);
45
46         if strfind(var, '*')==1 & isempty(end_element) ==
47             1
48             end_element=jj+start_element;
49         end
50     end
51
52     elements_data=input(start_element+1:end_element-1);
53     el_split= cell2mat(cellfun(@str2num, elements_data, '
54         uniform', 0)); %contains element nr + node 1-4
55
56 % Combine elements and nodes
57 clear ans ii jj fid var
58
59 elandnode = zeros(length(el_split), 9);
60 elandnode(:, 1)=el_split(:, 1);
61 for n=2:width(el_split)
62     for m=1:length(el_split)
63         k = find(el_split(m, n) == node_XY(:, 1));
64         elandnode(m, 2*n-2)=node_XY(k, 2);
65         elandnode(m, 2*n-1)=node_XY(k, 3);
66     end
67 end
68 clear m n k
69
70 %% Change the axis. For total image, the origin is top
71 left. For minmax_el,
72 %the origin is bottom left.
73 elandnode_img = zeros(length(elandnode), 9);
74 elandnode_img(:, 1) = elandnode(:, 1);
75 elandnode_img(:, 2) = size(total_image, 2)/2+elandnode(:, 2)
76 ;

```

```

73 elandnode_img(:,4) = size(total_image,2)/2+elandnode(:,4)
    ;
74 elandnode_img(:,6) = size(total_image,2)/2+elandnode(:,6)
    ;
75 elandnode_img(:,8) = size(total_image,2)/2+elandnode(:,8)
    ;
76
77 elandnode_img(:,3) = size(total_image,1)/2-elandnode(:,3)
    ;
78 elandnode_img(:,5) = size(total_image,1)/2-elandnode(:,5)
    ;
79 elandnode_img(:,7) = size(total_image,1)/2-elandnode(:,7)
    ;
80 elandnode_img(:,9) = size(total_image,1)/2-elandnode(:,9)
    ;
81
82
83 %% turn the element coordinates of relevant nodes into
    rect to crop
84 minmax_el=zeros(length(elandnode),5);
85 minmax_el(:,1)=el_split(:,1);
86 for i = 1:length(minmax_el)
87     minmax_el(i,2)=min(elandnode_img(i,[2 4 6 8])); %
        Min x
88     minmax_el(i,3)=min(elandnode_img(i,[3 5 7 9])); %
        min y
89     minmax_el(i,4)=max(elandnode_img(i,[2 4 6 8]))-min(
        elandnode_img(i,[2 4 6 8])); %width
90     minmax_el(i,5)=max(elandnode_img(i,[3 5 7 9]))-min(
        elandnode_img(i,[3 5 7 9])); %height
91 end
92 clear i
93
94 %% tilescan merged cut up in the elements:
95
96 source_filename = 'tilescan_105_8_cropped.png';
97
98 total_image = imread(source_filename); % Loads image
99
100 %% Get cropped images from total_image
101 %%make smaller cropped image
102 folder = 'C:\Users\bmeuser\Desktop\Maarten\Matlab
        tilescan\z10_elements\245_el\';
103 for i = 1:length(minmax_el)
104     rect = minmax_el(i,2:5);
105     Icropped = imcrop(total_image,rect);
106     name_base = 'element_%d.png';
107     name = sprintf(name_base,i);
108     name = append(folder,name);
109     imwrite(Icropped,name)

```

```

110 end
111
112 %% Find peak and kappa for all images/elements, and save
    in database.
113 % Takes a 15 min, as 1400 images need to be read out
    using several subfunctions
114 nbin=180;
115 scales          = [1.5, 2.5, 3.5];
116 threshold       = 0.9995;
117 showEachXArrow  = 1;
118
119 database = zeros(length(minmax_el),4); %contains 1
    element nr, 2 peak ang(deg), 3 kap, 4 fibre angles
    found
120 cd 'C:\Users\bmeuser\Desktop\Maarten\Matlab tilescan\
    z10_elements\94_el '
121 addpath 'C:\Users\bmeuser\Desktop\Maarten\Matlab tilescan
    ' ;
122 for iii = 1:length(minmax_el)
123     %Find what element we are in. All input except
        database updated every loop
124     name_vb = 'element_%d.png';
125     name_vb2 = sprintf(name_vb, iii);
126     match = ["element_" ".png"];
127     read_el = sscanf(erase(name_vb2,match), '%f'); %
        read_el is the current element nr we're looking at
128     database(iii,1) = read_el; %fill
        in database 1|: element nr.
129     im = imread(name_vb2);
130     im_green = im(:, :, 2);
131     im_green = im2double(im_green) .* 255;
132
133     try %When no angles are found, code gives error.
        Therefore try and catch
134         [ degrees, multiScaleHessian, vessMat, finalVess,
            dirs, pos] ...
135             = calcFibreOrient( im_green, scales,
                threshold);
136         phis = deg2rad(degrees)';
137         database(iii,4) = length(phis); %count the
            amount of fibre angles found in each element
            tile scan.
138         aparam = fib_estdist('phi', phis, 'nbin', nbin);
            % param = [mu sigma ani]
139         database(iii,2) = rad2deg(aparam(1)); %
            peak angleDatabase (2)
140         %find kap based on phis
141         d_ang = abs(phis-tparam(1)); %find the angle
            between the peak and the bins(so also

```

```

    individual fibres)
142 [d_n, d_bp]=fib_hist(d_ang, nbin);tot_surf=sum(
    d_n.*sin(d_bp)); %Conversion
143 conv = 2/tot_surf; %Conversion factor as found in
    HGO
144 n_c=d_n*conv;
145 database(iii,3) = 0.25.*sum(n_c.*sin(d_bp).^3);
146 catch %if no angles, database 2(peak) 3(kap) and 4 (
    angles). most safe.
147 degrees = 0;
148 database(iii,2) = 0;
149 database(iii,3) = 0.333;
150 database(iii,4) = 0;
151 disp('catch performed')
end
152
153 if database(iii,3) > 0.333
154     database(iii,3) = 0.333; %Calculate
        kappa =database (3)
155 else
156     %;
157 end
158 if database(iii,4)<100
159     database(iii,3)=0.333;
160 else
161     %;
162 end
163 end

1 function [ degrees, varargout] = calcFibreOrient( inImage
    , scales , threshold)
2 %calcFibreOrient: Main function for FOAtool, calculate
    all the results
3 %
4 % Example: degrees = calcFibreOrient( inImage, scales ,
    threshold)
5 % return the found orientations in degrees(0-180)
6 %
7 % Example:[ degrees, multiScaleHessian, vessMat,
    finalVess, dirs, pos] ...
8 % = calcFibreOrient( im_green, scales ,
    threshold);
9 % return the degrees and all the intermediary
    results
10 %
11 % Stefan Marien, 11/02/2016
12
13 imDims = size(inImage);
14
15 %% — Multiscale Hessian
16

```

```

17 % Pre-allocation
18 multiScaleHessian = zeros(size(inImage,1), size(
    inImage,2), size(scales,2), 3 );
19
20 % Loop through scales
21 for i = 1:size(scales,2)
22     multiScaleHessian(:,:,i,1) = gausSecDer(inImage,
    'xx', scales(i) );
23     multiScaleHessian(:,:,i,2) = gausSecDer(inImage,
    'xy', scales(i) );
24     multiScaleHessian(:,:,i,3) = gausSecDer(inImage,
    'yy', scales(i) );
25 end
26
27 %% — Pixelwise vesselness calculation by eigenvalue
    decomposition
28
29 % Pre-allocation
30 vessMat = zeros(size(multiScaleHessian, 1), size(
    multiScaleHessian, 2), size(multiScaleHessian, 3)
    );
31 eigVecs = zeros(size(multiScaleHessian, 1), size(
    multiScaleHessian, 2), size(multiScaleHessian, 3),
    2);
32
33 % Loop through each scale
34 for iScale = 1:size(scales,2)
35
36     % Calculate c value for each image (see
        vesselness formula)
37     hessNorms = sqrt( multiScaleHessian(:,:,iScale,1)
        .^2 + multiScaleHessian(:,:,iScale,2).^2 +
        multiScaleHessian(:,:,iScale,3).^2 ) ;
38     cValue = 0.5 * max( abs( hessNorms(:) ) );
39
40 % Loop through image
41 for y = 1:imDims(2)
42     for x = 1:imDims(1)
43
44         % Reconstruct Hessian mat (form row to
            mat)
45         curHessMat = [ multiScaleHessian(x,y,
            iScale,1), multiScaleHessian(x,y,
            iScale,2);
46
            multiScaleHessian(x,y,
            iScale,2),
            multiScaleHessian(x,y,
            iScale,3) ];
47
48         % Calculate frangi vesselness value

```

```

49         [vess , eigVec] = calcFrangiVesselness(
50             curHessMat , cValue);
51         vessMat(x,y,iScale) = vess;
52
53         % Save largest eigenvectors (principal
54         % direction)
55         eigVecs(x,y,iScale,:) = eigVec;
56     end
57 end
58
59 %% — Select maximum vesselness across scales
60 bestScales = zeros(size(multiScaleHessian,1),size(
61     multiScaleHessian,2));
62
63 for y = 1:imDims(2)
64     for x = 1:imDims(1)
65
66         % Find scale with highest vesselness, 'last'
67         % makes it take the
68         % highest scale when several scales have the
69         % same vesselness
70         maxVes = max(vessMat(x,y,:));
71         bestScales(x,y) = find(vessMat(x,y,:) ==
72             maxVes, 1, 'last');
73     end
74 end
75
76 % Build vesselness image
77 finalVess = max(vessMat, [], 3);
78
79 % Threshold vesselness image
80 finalVessThres = im2bw(finalVess, threshold) .*
81     finalVess;
82
83 %% — Extract directions after threshold
84
85 % Pre-allocation
86 dirs = zeros(2, sum(finalVessThres(:) > 0.995));
87 pos = zeros(2, sum(finalVessThres(:) > 0.995));
88 counter = 1;
89
90 % Loop through image
91 for y = 1:imDims(2)
92     for x = 1:imDims(1)
93
94         % Use only pixels from thresholded vesselness
95         % image

```

```

91         if finalVessThres(x,y) > 0
92             % Get best scale
93             iScale = bestScales(x,y);
94             % Export to list variables
95             dirs(:,counter) = [ eigVecs(x,y,iScale,2)
96                 ; eigVecs(x,y,iScale,1) ];
97             pos(:,counter) = [x ; y];
98             counter = counter + 1;
99         end
100     end
101 end
102
103 %% — Orientation statistics
104
105 % Pre-allocation
106 degrees = zeros(1, size(pos,2));
107
108 % Loop though each vessel pixel
109 for i = 1:size(pos,2)
110     % Calculate angle
111     degrees(i) = atan2d( dirs(1,i), dirs(2,i) );
112
113     % Combine into 180 degree range
114     if degrees(i) >= 180
115         degrees(i) = degrees(i) - 180;
116
117     elseif degrees(i) <= 0
118         degrees(i) = degrees(i) + 180;
119
120     end
121 end
122
123 % Handle optional out arguments
124 if nargin~=1
125     varargout{1} = multiScaleHessian ;
126     varargout{2} = vessMat ;
127     varargout{3} = finalVess ;
128     varargout{4} = dirs ;
129     varargout{5} = pos ;
130     varargout{6} = degrees ;
131 end
132 end

```

```

1  function [start_node ,start_element ,end_element ,
      start_elsetPLAQUE ,end_elsetPLAQUE, start_materials ,
      end_part] = FindInputSections(filename)
2
3  % Read input file text
4  fid = fopen(filename , 'r');
5  input = textscan(fid , '%s' , 'delimiter' , '\n');
6  input = lower(input{1}); % Using lower() makes the
      input lower-case ,
7  fclose(fid); % so that I don't need to
      worry about
8
9  % case-sensitivity
10
11 % Pre-allocate variables
12 start_node = [];
13 start_element = [];
14 end_element = [];
15 start_elsetPLAQUE = [];
16 start_materials = [];
17 end_part = [];
18
19 %% Run through lines to find the desired section headers
20 for ii=1:length(input)
21     var=input{ii};
22     var=strtrim(var);
23
24     if strfind(var , '*node')==1 & isempty(start_node)
25         == 1
26         start_node=ii;
27     end
28
29     if strfind(var , '*element')==1 & isempty(
30         start_element) == 1
31         start_element=ii;
32     end
33
34     if strfind(var , '*elset , elset=set-1') == 1 &
35         isempty(start_elsetPLAQUE) == 1
36         start_elsetPLAQUE=ii;
37     end
38
39     if strfind(var , '** materials') == 1 & isempty(
40         start_materials) == 1
41         start_materials=ii;
42     end
43
44     if strfind(var , '*end part') == 1 & isempty(
45         end_part) == 1
46         end_part=ii;

```

```

42         end
43     end
44
45     %% Run through input to find desired section ends
46     % end_element
47     fid = fopen(filename, 'r');
48     input_afterelements = textscan(fid, '%s', 'Delimiter', '\n',
49     'HeaderLines', start_element);
50     fclose(fid);
51
52     for jj = 1:length(input_afterelements)
53         var=input_afterelements{jj};
54         var=strtrim(var);
55
56         if strfind(var, '*')==1 & isempty(end_element) ==
57             1
58             end_element=jj+start_element;
59         end
60     end
61     % end_elsetPLAQUE
62     fid = fopen(filename, 'r');
63     input_afterelsetPLAQUE = textscan(fid, '%s', 'Delimiter', '\n',
64     'HeaderLines', start_elsetPLAQUE);
65     end_elsetPLAQUE = input_afterelsetPLAQUE{1};
66     fclose(fid);
67
68     for kk = 1:length(input_afterelsetPLAQUE)
69         var=input_afterelsetPLAQUE{kk};
70         var=strtrim(var);
71
72         if strfind(var, '*')==1 & isempty(end_elsetPLAQUE) ==
73             1
74             end_elsetPLAQUE=kk+start_elsetPLAQUE;
75         end
76     end
77 end

```

```

1 function [node_coordinates] = NodeCoordinates(
2     input_filename, start_node, start_element)
3 fid = fopen(input_filename); % Open .inp file and save
4     fileID
5     formatSpec = '%f%f%f'; % Define format for
6     ABAQUS .inp file
7     % node definitions

```

```
7 % Extract text-data from node section of the .inp file
8 dataArray = textscan(fid, formatSpec, start_element-(
    start_node+1), 'Delimiter', ',', 'EmptyValue', NaN,
    'HeaderLines', start_node, 'ReturnOnError', false);
9
10 % Define the node coordinates
11 node_coordinates = [dataArray{1:end}];
12
13 fclose(fid)
14 end
```

Appendix B

Appendix B contains the Matlab code required to calculate the fibre organisation, based on the 6 datasets created from the tilescan.

Matlab Code

```
1 close all
2 clc
3
4 el_core =[minmax_el(:,2)+0.5*minmax_el(:,4) minmax_el
           (:,3)+0.5*minmax_el(:,5)]; %Find the centre of the
           elements approximately
5 el_core(:,2) = 4219-el_core(:,2);
6 %sz = (10*database(:,4)+mean(database(:,4)))/10; %
           amount of angles, averaged with the mean
7 %scat_a0 = scatter(el_core(:,1),el_core(:,2),sz,database
           (:,3),'filled');
8 %set(gca,'YDir','reverse')
9 %hold on
10 %quiver(el_core(:,1),el_core(:,2),cosd(angle_tilescan),
           sind(angle_tilescan));
11
12 %% compare the three tilescans in angle amount
13 %database_z8 = database; Run tilescan_calc for each
           database seperately.
14 %database_z9 = database;
15 %database_z10 = database;
16
17 database_tot_94_ang = zeros(length(minmax_el),4);
18 database_tot_94_ang(:,1)=database(:,1);
19 for i =1:length(database)
20     database_tot_94_ang(i,4)= max([database_z8_94(i,4)
           database_z9_94(i,4) database_z10_94(i,4)]);
21     if database_tot_94_ang(i,4)== database_z8_94(i,4)
22         database_tot_94_ang(i,3)=database_z8_94(i,3);
23         database_tot_94_ang(i,2)=database_z8_94(i,2);
24     elseif database_tot_94_ang(i,4)== database_z9_94(i,4)
25         database_tot_94_ang(i,3)=database_z9_94(i,3);
26         database_tot_94_ang(i,2)=database_z9_94(i,2);
27     else
28         database_tot_94_ang(i,3)=database_z10_94(i,3);
29         database_tot_94_ang(i,2)=database_z10_94(i,2);
30     end
31 end
32
33 %% Compare the tilescans on lowest kappa
34 database_tot_245_kap = zeros(length(database_z10_245),4);
35 database_tot_245_kap(:,1)=database_z10_245(:,1);
```

```

36 for i =1:length(database)
37     database_tot_245_kap(i,3)= min([ database_z8_245(i,3)
38         database_z9_245(i,3) database_z10_245(i,3) ]);
39     if database_tot_245_kap(i,3)== database_z8_245(i,3)
40         database_tot_245_kap(i,4)=database_z8_245(i,4);
41         database_tot_245_kap(i,2)=database_z8_245(i,2);
42     elseif database_tot_245_kap(i,3)== database_z9_245(i
43         ,3)
44         database_tot_245_kap(i,4)=database_z9_245(i,4);
45         database_tot_245_kap(i,2)=database_z9_245(i,2);
46     else
47         database_tot_245_ang(i,4)=database_z10_245(i,4);
48         database_tot_245_ang(i,2)=database_z10_245(i,2);
49     end
50 end
51 %% get angles for quiver of database total
52 angle_tilscan= zeros(length(database_tot_94_ang(:,2)),1)
53 ;
54 for i = 1: length(database_tot_94_ang)
55     if database_tot_94_ang(i,2) <=90
56         angle_tilscan(i) = database_tot_94_ang(i,2);
57     else
58         angle_tilscan(i)=database_tot_94_ang(i,2)-180;
59     end
60 end
61 %% plot
62 close all
63 clc
64 el_core(:,1) = 1:94
65 el_core(:,2) = 1:94
66 sz = (10*database_tot_94_ang(:,4)+mean(
67     database_tot_94_ang(:,4)))/120; %amount of angles,
68     averaged with the mean
69 %colours = [3*database_tot_94_ang(:,3) 0*
70     database_tot_94_ang(:,3) 1-database_tot_94_ang(:,3)];
71 %scat_a0 = scatter(el_core(:,1),el_core(:,2),sz,
72     database_tot_94_ang(:,3), 'filled');
73 scat1 = scatter(el_core(:,1),el_core(:,2),400,
74     database_tot_94_ang(:,3), 'filled');
75 title('\kappa over 94 elements depth 119 \mum')
76 set(gcf, 'Position',[200 200 600 600]);
77 %set(gca, 'YDir', 'reverse')
78 %hold on
79 %quiver(el_core(:,1),el_core(:,2),cosd(
80     database_tot_94_ang(:,2)).*(0.333-database_tot_94_ang
81     (:,3)),sind(database_tot_94_ang(:,2)).*(0.333-
82     database_tot_94_ang(:,3)));
83
84

```

```

75 %% Top right
76 close all
77 sz = (10*database_tot_94_ang(1:21,4)+mean(
    database_tot_94_ang(1:21,4)))/60; %amount of
    angles, averaged with the mean
78 scat_a0 = scatter(el_core94(1:21,1),el_core94(1:21,2)
    ,1200,database_tot_94_ang(1:21,3),'filled');
79 %set(gca,'YDir','reverse')
80 hold on
81 quiver(el_core94(1:21,1),el_core94(1:21,2),cosd(
    database_tot_94_ang(1:21,2)).*(0.333-
    database_tot_94_ang(1:21,3)),sind(database_tot_94_ang
    (1:21,2)).*(0.333-database_tot_94_ang(1:21,3)));
82 %text(el_core(1:57,1),el_core(1:57,2),database_tot_94_ang
    (1:57,1));
83 set(gcf,'Position',[200 200 600 600]);
84
85 %% Top right 245
86 close all
87 scat_a0 = scatter(el_core245(1:57,1),el_core245(1:57,2)
    ,700,database_tot_245_ang(1:57,3),'filled');
88 %set(gca,'YDir','reverse')
89 hold on
90 quiver(el_core245(1:57,1),el_core245(1:57,2),cosd(
    database_tot_245_ang(1:57,2)).*(0.333-
    database_tot_245_ang(1:57,3)),sind(
    database_tot_245_ang(1:57,2)).*(0.333-
    database_tot_245_ang(1:57,3)));
91 set(gcf,'Position',[200 200 600 600]);
92
93 %% plot losse graphs voor thesis
94 close all
95 clc
96 sz = (10*database_z9_94(:,4)+mean(database_z9_94(:,4)))
    /120; %amount of angles, averaged with the mean
97 %colours = [3*database_tot_94_ang(:,3) 0*
    database_tot_94_ang(:,3) 1-database_tot_94_ang(:,3)];
98 %scat_a0 = scatter(el_core(:,1),el_core(:,2),sz,
    database_tot_94_ang(:,3),'filled');
99 scat1 = scatter(el_core(:,1),el_core(:,2),400,
    database_z9_94(:,3),'filled');
100 title('\kappa over 94 elements depth 119 \mum')
101 set(gcf,'Position',[200 200 800 600]);
102 xlabel('x coordinates [pix]')
103 ylabel('y coordinates [pix]')
104 %set(gca,'YDir','reverse')
105 %hold on
106 %quiver(el_core(:,1),el_core(:,2),cosd(
    database_tot_94_ang(:,2)).*(0.333-database_tot_94_ang
    (:,3)),sind(database_tot_94_ang(:,2)).*(0.333-

```

```

        database_tot_94_ang(:,3));
107 %%
108 close all
109 clc
110 tiledlayout(3,2)
111 size=200;
112 set(gcf, 'Position',[100 100 1000 900]);
113 nexttile
114 scat1 = scatter(el_core94(:,1),el_core94(:,2),size,
        database_z8_94(:,3), 'filled');
115 title('\kappa over 94 elements depth 105 \mum')
116 %set(gcf, 'Position',[200 200 800 600]);
117
118
119 nexttile
120 scat1 = scatter(el_core245(:,1),el_core245(:,2),size*0.5,
        database_z8_245(:,3), 'filled');
121 title('\kappa over 245 elements depth 105 \mum')
122 %set(gcf, 'Position',[200 200 800 600]);
123
124
125 nexttile
126 scat1 = scatter(el_core94(:,1),el_core94(:,2),size,
        database_z9_94(:,3), 'filled');
127 title('\kappa over 94 elements depth 119 \mum')
128 %
129 %xlabel('x coordinates [pix]')
130 %ylabel('y coordinates [pix]')
131
132
133 nexttile
134 scat1 = scatter(el_core245(:,1),el_core245(:,2),size*0.5,
        database_z9_245(:,3), 'filled');
135 title('\kappa over 245 elements depth 119 \mum')
136 %set(gcf, 'Position',[200 200 100 80]);
137
138 nexttile
139 scat1 = scatter(el_core94(:,1),el_core94(:,2),size,
        database_z10_94(:,3), 'filled');
140 title('\kappa over 94 elements depth 135 \mum')
141 %set(gcf, 'Position',[200 200 800 600]);
142
143
144 nexttile
145 scat1 = scatter(el_core245(:,1),el_core245(:,2),size*0.5,
        database_z10_245(:,3), 'filled');
146 title('\kappa over 245 elements depth 135 \mum')
147 %set(gcf, 'Position',[200 200 800 600]);
148
149 %% scatter en quiver total 94 en 245

```

```

150 close all
151 clc
152 tiledlayout(1,2)
153 size=200;
154 set(gcf, 'Position',[100 100 1300 600]);
155 nexttile
156 scat1 = scatter(el_core94(:,1),el_core94(:,2),1.5*size,
    database_tot_94_ang(:,3), 'filled');
157 title('\kappa and a_0 over 94 elements')
158 hold on
159 quiver(el_core94(:,1),el_core94(:,2),cosd(
    database_tot_94_ang(:,2)).*(0.333-database_tot_94_ang
    (:,3)),sind(database_tot_94_ang(:,2)).*(0.333-
    database_tot_94_ang(:,3)));
160
161 nexttile
162 scat1 = scatter(el_core245(:,1),el_core245(:,2),size,
    database_tot_245_ang(:,3), 'filled');
163 title('\kappa and a_0 over 245 elements')
164 hold on
165 quiver(el_core245(:,1),el_core245(:,2),cosd(
    database_tot_245_ang(:,2)).*(0.333-
    database_tot_245_ang(:,3)),sind(database_tot_245_ang
    (:,2)).*(0.333-database_tot_245_ang(:,3)));
166
167 %%
168 close all
169 clc
170 tiledlayout(1,2)
171 size=40;
172 set(gcf, 'Position',[100 100 1400 600]);
173 nexttile
174 quiver(el_core(:,1),el_core(:,2),cosd(ang_samp4(:,2)),
    sind(ang_samp4(:,2)))
175 title('a_0 sample 4')
176
177 nexttile
178 scatter(el_core(:,1),el_core(:,2),size,kap_samp4s(:,2),
    'filled');
179 title('\kappa sample 4')
180
181 %% quiver plots all 6
182 close all
183 clc
184 minmax_el=zeros(length(elandnode),5);
185 minmax_el(:,1)=elandnode(:,1);
186 for i = 1:length(minmax_el)
187     minmax_el(i,2)=min(elandnode(i,[2 4 6 8])); %Min
    x

```

```

188     minmax_el(i,3)=min(elandnode(i,[3 5 7 9]));    %min
        y
189     minmax_el(i,4)=max(elandnode(i,[2 4 6 8]))-min(
        elandnode(i,[2 4 6 8])); %width
190     minmax_el(i,5)=max(elandnode(i,[3 5 7 9]))-min(
        elandnode(i,[3 5 7 9])); %height
191 end
192 %%
193 close all
194 set(gcf,'Position',[100 100 700 800]);
195 quiver(el_core(:,1),el_core(:,2),cosd(database_z10_245
        (:,2)),sind(database_z10_245(:,2)))
196 title('a_0 at 245 elements at depth of 135 \mu m ')

```

Appendix C

Appendix C contains the Matlab code required to build the ABAQUS input files for the anisotropic simulations. The first code determines the local fibre orientation. The second script calculates the used fibre dispersion input. The third code is used to write the ABAQUS input file. The code for sample 1 is given.

Matlab Code

```
1 %% Angles per group, based on sample elements
2 %Groups
3 A1 = [647:742]';
4 A2 = [998:1085]';
5 A3 = [944:997]';
6 A5 = [631:646]';
7
8 B1 = [1418:1509]';
9 B2 = [1542:1637]';
10 B5 = [1510:1541]';
11
12 T6 = [551:630]';
13 B6 = [1158:1273]';
14 R1 = [1086:1157]';
15 R2 = [1274:1417]';
16 L1 = [109:172]';
17 L2 = [407:550]';
18
19 C1 = [290:406]';
20 C2 = [779:895]';
21 C3 = [896:943]';
22 C5 = [743:778]';
23
24 D1 = [1:108]';
25 D2 = [173:271]';
26 D5 = [272:289]';
27
28
29 %%
30 clc
31 ang_samp3 = zeros(length(elandnode),2);
32 ang_samp3(:,1)=elandnode(:,1);
33
34 minmax_el=zeros(length(elandnode),5);
35 minmax_el(:,1)=elandnode(:,1);
36 for i = 1:length(minmax_el)
37     minmax_el(i,2)=min(elandnode(i,[2 4 6 8])); %Min
38     x
```

```

38     minmax_el(i,3)=min(elandnode(i,[3 5 7 9])); %min
39     y
40     minmax_el(i,4)=max(elandnode(i,[2 4 6 8]))-min(
41     elandnode(i,[2 4 6 8])); %width
42     minmax_el(i,5)=max(elandnode(i,[3 5 7 9]))-min(
43     elandnode(i,[3 5 7 9])); %height
44 end
45 el_core =[minmax_el(:,2)+0.5*minmax_el(:,4) minmax_el
46     (:,3)+0.5*minmax_el(:,5)];
47 %% calc angles 1,2,3 (A,B C D)
48 cur= L2;
49 close all
50 for i = min(cur):max(cur) %For each element the x and
51     y coordinates are calculated of the 2 edge nodes,
52     leading to an angle.
53     x_A1=sort(elandnode(i,[2 4 6 8]),2); %Per element,
54     find the four relevant nodes, and sort them
55     ascending
56     dx_A1 =x_A1(2)-x_A1(1); %the two nodes with
57     max X are chosen and subtracted
58     n1 = find(elandnode(i,[2 4 6 8])==x_A1(2)); %Node
59     number with the highest x
60     n2 = find(elandnode(i,[2 4 6 8])==x_A1(1)); %Node
61     number with second highest x
62     dy_A1=elandnode(i,1+2*n1)-elandnode(i,1+2*n2); %
63     Find dY of two selected nodes
64     if dx_A1 == 0
65         ang_samp3(i,2) = 90;
66     else
67         ang_samp3(i,2) = atand(dy_A1/dx_A1);
68     end
69 end
70 quiver(el_core(cur,1),el_core(cur,2),cosd(ang_samp3(cur
71     ,2)),sind(ang_samp3(cur,2)))
72 set(gcf,'Position',[100 100 600 800])
73 %% false angles change
74 %Noteren welke angles fout:
75 %A1: 695:722
76 %A2: -
77 %B1: 1418:1432 1447:1461
78 %B2: -
79 %R1: -
80 %R2:
81 %C3: 935:943 896:903
82
83 %A3: 989:927 - 991,994 986 983 954:958 952
84 %C1: 291:302 339:374

```

```

75 %C2: -
76 %D1: 17:32 77:108 14:16 11:12
77 %D2:-
78 %L1:-
79 %L2: 487
80 %extra
81 for i = 487 %For each element the x and y coordinates are
      calculated of the 2 edge nodes, leading to an angle.
82   x_A1=sort(elandnode(i,[2 4 6 8]),2); %Per element,
      find the four relevant nodes, and sort them
      ascending
83   dx_A1 =x_A1(1)-x_A1(3); %the two nodes with
      max X are chosen and subtracted
84   n1 = find(elandnode(i,[2 4 6 8])==x_A1(1)); %Node
      number with the chosen x: 1 is lowest x, 4 is
      highest
85   n2 = find(elandnode(i,[2 4 6 8])==x_A1(3)); %Node
      number with second chosen x 1 is lowest x, 4 is
      highest
86   dy_A1=elandnode(i,1+2*n1)-elandnode(i,1+2*n2); %
      Find dY of two selected nodes
87   if dx_A1 == 0
88     ang_samp3(i,2) = 90;
89   else
90     ang_samp3(i,2) = atand(dy_A1/dx_A1);
91   end
92 end
93
94 quiver(el_core(cur,1),el_core(cur,2),cosd(ang_samp3(cur
      ,2)),sind(ang_samp3(cur,2)))
95 set(gcf,'Position',[100 100 600 800])
96
97 %% A-D 4-6, all angles are 90 deg:
98
99 %ang_samp3(A4,2)=90;
100 ang_samp3(A5,2)=90;
101
102 %ang_samp3(B4,2)=90;
103 ang_samp3(B5,2)=90;
104
105 %ang_samp3(C4,2)=90;
106 ang_samp3(C5,2)=90;
107
108 %ang_samp3(D4,2)=90;
109 ang_samp3(D5,2)=90;
110
111 ang_samp3(T6,2)=90;
112 ang_samp3(B6,2)=90;
113
114 ang_samp3(L2,2)=90;

```

```

115 ang_samp3(R2,2)=90;
116
117 quiver(el_core(:,1),el_core(:,2),cosd(ang_samp3(:,2)),
        sind(ang_samp3(:,2)))
118 %% from -90 to +90 to 0-180
119
120 for i = 1:length(ang_samp3)
121     if ang_samp3(i,2)<0
122         ang_samp3(i,2) = ang_samp3(i,2)+180;
123     end
124 end
125
126 %% kappas of sample 1 per element
127 kap_samp3 = zeros(length(elandnode),2);
128 kap_samp3(:,1) = elandnode(:,1);
129 kap1 = 0.263;
130 kap2 = 0.298;
131 kap3 = 0.298;
132 kap4 = 0.306;
133 kap5 = 0.317;
134 kap6 = 0.333;
135 kap_samp3([A1',B1', C1',D1',R1',L1'],2)=kap1;
136 kap_samp3([A2',B2', C2',D2',R2',L2'],2)=kap2;
137 kap_samp3([A3', C3'],2)=kap3;
138 %kap_samp3([A4', B4', C4', D4'],2)=kap4;
139 kap_samp3([A5', B5', C5', D5'],2)=kap5;
140 kap_samp3([T6', B6'],2)=kap6;

1 %% Calculate kappa's per group
2 %%94 ele
3 clc
4 kap1 = database_tot_94_ang(1:21,3);    %kap1 is the
        kappas from element 1:21 based on the maximum angle
        amount
5 kap2 = database_tot_94_kap(1:21,3);    %kap2 based on
        min kap.
6 ang1 = database_tot_94_ang(1:21,2);
7 ang2 = database_tot_94_kap(1:21,2);
8
9 kap3 = database_tot_245_ang(1:57,3);    %kap1 is the
        kappas from element 1:57 based on the maximum angle
        amount
10 kap4 = database_tot_245_kap(1:57,3);    %kap2 based on
        min kap.
11 ang3 = database_tot_245_ang(1:57,2);
12 ang4 = database_tot_245_kap(1:57,2);
13
14 %groups 94 ele
15 g11 = [1 2 10 13];
16 g12 = [3 4 9 12];

```

```

17 g13 = [7 8 20];
18 g14 = [5 6 16 18];
19 g15 = [11 14];
20 g16 = [15 17 19 21];
21
22 %groups 245 ele
23 g21 = [1 2 3 4 5 6 7 8 9 10 36 37 42 43];
24 g22 = [11 12 13 14 15 16 17 18 19 20 34 35];
25 g23 = [29 30 31 32 33 54 56];
26 g24 = [21 22 23 24 25 26 27 28 46 48 50 52];
27 g25 = [38 39 40 41 44];
28 g26 = [45 47 49 51 53 55 57];
29
30 %Kappa based on max ang (kap 1) for 94 elements (g1)
31 kap1g11 = mean(kap1(g11)); %kap11=kap21
32 kap1g12 = mean(kap1(g12));
33 kap1g13 = mean(kap1(g13));
34 kap1g14 = mean(kap1(g14));
35 kap1g15 = mean(kap1(g15));
36 kap1g16 = mean(kap1(g16));
37
38 %kappa based on min kap (kap2) for 94 elements (g1)
39 kap2g11 = mean(kap2(g11)); %kap11=kap21
40 kap2g12 = mean(kap2(g12));
41 kap2g13 = mean(kap2(g13));
42 kap2g14 = mean(kap2(g14));
43 kap2g15 = mean(kap2(g15));
44 kap2g16 = mean(kap2(g16));
45
46 %Kappa based on max ang (kap 1) for 245 elements (g2)
47 kap3g21 = mean(kap3(g21)); %kap11=kap21
48 kap3g22 = mean(kap3(g22));
49 kap3g23 = mean(kap3(g23));
50 kap3g24 = mean(kap3(g24));
51 kap3g25 = mean(kap3(g25));
52 kap3g26 = mean(kap3(g26));
53
54 %kappa based on min kap (kap2) for 245 elements (g2)
55 kap4g21 = mean(kap4(g21)); %kap11=kap21
56 kap4g22 = mean(kap4(g22));
57 kap4g23 = mean(kap4(g23));
58 kap4g24 = mean(kap4(g24));
59 kap4g25 = mean(kap4(g25));
60 kap4g26 = mean(kap4(g26));
61
62 kap1_tot = [kap1g11 kap2g11 kap3g21 kap4g21];
63 kap2_tot = [kap1g12 kap2g12 kap3g22 kap4g22];
64 kap3_tot = [kap1g13 kap2g13 kap3g23 kap4g23];
65 kap4_tot = [kap1g14 kap2g14 kap3g24 kap4g24];
66 kap5_tot = [kap1g15 kap2g15 kap3g25 kap4g25];

```

```

67 kap6_tot = [kap1g16 kap2g16 kap3g26 kap4g26];
68
69 kap_tot = [kap1_tot; kap2_tot; kap3_tot; kap4_tot;
             kap5_tot ;kap6_tot]; %Shows kappa per 4 methods. They
             are very similar. So it works.
70
71 %% Angles per group, based on sample elements
72 %Groups
73 A1 = [21:46]';
74 A2 = [1:20]';
75 A3 = [87:93]';
76 A4 = [59:86]';
77 A5 = [47:58]';
78 T6 = [213:242]';
79 B6 = [345:380]';
80
81 B1 = [116:146]';
82 B2 = [94:115]';
83 B3 = [243:246]';
84 B4 = [247:276]';
85 B5 = [277:281]';
86
87 C1 = [282:318]';
88 C2 = [391:412]';
89 C3 = [413:417]';
90 C4 = [418:444]';
91 C5 = [381:390]';
92
93 D1 = [147:181]';
94 D2 = [319:338]';
95 D3 = [339:344]';
96 D4 = [192:212]';
97 D5 = [182:191]';
98
99 %% calc angles
100 clc
101 ang_samp1 = zeros(length(elandnode),2);
102 ang_samp1(:,1)=elandnode(:,1);
103 for i = min(A1):max(A1) %For each element the x and y
             coordinates are calculated of the 2 edge nodes,
             leading to an angle.
104     x_A1=sort(elandnode(i,[2 4 6 8]),2); %Per element,
             find the four relevant nodes, and sort them
             ascending
105     dx_A1 =x_A1(4)-x_A1(3); %the two nodes with
             max X are chosen and subtracted
106     n1 = find(elandnode(i,[2 4 6 8])==x_A1(4)); %Node
             number with the highest x
107     n2 = find(elandnode(i,[2 4 6 8])==x_A1(3)); %Node
             number with second highest x

```

```

108     dy_A1=elandnode(i,1+2*n1)-elandnode(i,1+2*n2);    %
        Find dY of two selected nodes
109     if dx_A1 == 0
110         ang_samp1(i,2) = 90;
111     else
112         ang_samp1(i,2) = atand(dy_A1/dx_A1);
113     end
114
115 end
116 ang_samp1(25,2) = 33.0145;%1 error at element 25, since
        the lowest node has lower x than the top one
117
118 %% A1, A2, B1,B2, C3, D3
119 for i = min(D3):max(D3)    %For each element the x and y
        coordinates are calculated of the 2 edge nodes,
        leading to an angle.
120     x_A2=sort(elandnode(i,[2 4 6 8]),2);    %Per element,
        find the four relevant nodes, and sort them
        ascending
121     dx_A2 =x_A2(4)-x_A2(3);    %the two nodes with
        max X are chosen and subtracted
122     n1 = find(elandnode(i,[2 4 6 8])==x_A2(4)); %Node
        number with the highest x
123     n2 = find(elandnode(i,[2 4 6 8])==x_A2(3)); %Node
        number with second highest x
124     dy_A2=elandnode(i,1+2*n1)-elandnode(i,1+2*n2);    %
        Find dY of two selected nodes
125     if dx_A2 == 0
126         ang_samp1(i,2) = 90;
127     else
128         ang_samp1(i,2) = atand(dy_A2/dx_A2);
129     end
130
131 end
132
133 plot(ang_samp1(min(D3):max(D3),1),ang_samp1(min(D3):max(
        D3),2))
134 %% Edit wrong angles using different angles.
135 %wrongB1= [116 117 118 121:126 128]';    %Use the third
        node instead of the second
136 % wrongC1 =[283:285 309:318]' use 1 and 3
137 %Wrong D1 = 154:158, use 1 and 3
138 for i = 282    %For each element the x and y coordinates
        are calculated of the 2 edge nodes, leading to an
        angle.
139     x_A1=sort(elandnode(i,[2 4 6 8]),2);    %Per element,
        find the four relevant nodes, and sort them
        ascending
140     dx_A1 =x_A1(3)-x_A1(1);    %the two nodes with
        max X are chosen and subtracted

```

```

141     n1 = find(elandnode(i,[2 4 6 8])==x_A1(2)); %Node
        number with the highest x
142     n2 = find(elandnode(i,[2 4 6 8])==x_A1(1)); %Node
        number with second highest x
143     dy_A1=elandnode(i,1+2*n1)-elandnode(i,1+2*n2); %
        Find dY of two selected nodes
144     if dx_A1 == 0
145         ang_samp1(i,2) = 90;
146     else
147         ang_samp1(i,2) = atand(dy_A1/dx_A1);
148     end
149 end
150 ang_samp1(116,2)=-60;
151 ang_samp1(120,2)=-60; %! angle won't work
152 ang_samp1(285:286,2)=60; %! angle won't work
153 ang_samp1(317:318,2)=60;
154 ang_samp1(147:153,2)=-30;
155 ang_samp1(163,2)=-30;
156
157 %% C1,C2, D1, D2, A3,B3
158 for i = min(B3):max(B3) %For each element the x and y
        coordinates are calculated of the 2 edge nodes,
        leading to an angle.
159     x_A1=sort(elandnode(i,[2 4 6 8]),2); %Per element,
        find the four relevant nodes, and sort them
        ascending
160     dx_A1 =x_A1(2)-x_A1(1); %the two nodes with
        max X are chosen and subtracted
161     n1 = find(elandnode(i,[2 4 6 8])==x_A1(2)); %Node
        number with the lowest x
162     n2 = find(elandnode(i,[2 4 6 8])==x_A1(1)); %Node
        number with second lowest x
163     dy_A1=elandnode(i,1+2*n1)-elandnode(i,1+2*n2); %
        Find dY of two selected nodes
164     if dx_A1 == 0
165         ang_samp1(i,2) = 90;
166     else
167         ang_samp1(i,2) = atand(dy_A1/dx_A1);
168     end
169 end
170 plot(ang_samp1(min(B3):max(B3),1),ang_samp1(min(B3):max(
        B3),2))
171
172 %% A-D 4-6, all angles are 90 deg:
173 ang_samp1(A4,2)=90;
174 ang_samp1(A5,2)=90;
175
176 ang_samp1(B4,2)=90;
177 ang_samp1(B5,2)=90;
178

```

```

179 ang_samp1(C4,2)=90;
180 ang_samp1(C5,2)=90;
181
182 ang_samp1(D4,2)=90;
183 ang_samp1(D5,2)=90;
184
185 ang_samp1(T6,2)=90;
186 ang_samp1(B6,2)=90;
187
188 %% make check quiver for angles
189 minmax_el=zeros(length(elandnode),5);
190 minmax_el(:,1)=elandnode(:,1);
191 for i = 1:length(minmax_el)
192     minmax_el(i,2)=min(elandnode(i,[2 4 6 8])); %Min
193     minmax_el(i,3)=min(elandnode(i,[3 5 7 9])); %min
194     minmax_el(i,4)=max(elandnode(i,[2 4 6 8]))-min(
195         elandnode(i,[2 4 6 8])); %width
196     minmax_el(i,5)=max(elandnode(i,[3 5 7 9]))-min(
197         elandnode(i,[3 5 7 9])); %height
198 end
199 el_core =[minmax_el(:,2)+0.5*minmax_el(:,4) minmax_el
200           (:,3)+0.5*minmax_el(:,5)];
201 quiver(el_core(:,1),el_core(:,2),cosd(ang_samp1(:,2)),
202        sind(ang_samp1(:,2)))
203
204 %% from -90 to +90 to 0-180
205
206 for i = 1:length(ang_samp1)
207     if ang_samp1(i,2)<0
208         ang_samp1(i,2) = ang_samp1(i,2)+180;
209     end
210 end
211
212 %% kappas of sample 1 per element
213 kap_samp1 = zeros(length(elandnode),2);
214 kap_samp1(:,1) = elandnode(:,1);
215 kap1 = 0.263;
216 kap2 = 0.298;
217 kap3 = 0.298;
218 kap4 = 0.306;
219 kap5 = 0.317;
220 kap6 = 0.333;
221 kap_samp1([A1', B1', C1', D1'],2)=kap1;
222 kap_samp1([A2', B2', C2', D2'],2)=kap2;
223 kap_samp1([A3', B3', C3', D3'],2)=kap3;
224 kap_samp1([A4', B4', C4', D4'],2)=kap4;
225 kap_samp1([A5', B5', C5', D5'],2)=kap5;
226 kap_samp1([T6', B6'],2)=kap6;

```

```

1 %% run tilescan_calc for the kappa and a0.
2 %Base the kappa and a0 in the inp file on tilescan first.
3 %Then base the kappa and a0 input for the new inp file on
4   the ang_cut_aba,
5 %so the stress from the abaqus .rpt file
6
7 new_filename = 'samplxfem.mb.inp';
8 input_filename = 'samplxfem.inp';
9
10 % HGO Material Parameters
11 C10 = '0.05'; %zou dit wat uitmaken? van 0.05 naar 0.25
12   ook niet
13 D = '0';
14 k1 = '26';
15 k2 = '2.5';
16 dmg_init='0.3'; %terug naar 0.3 ipv 0.25 Dat is goed,
17   maakt geen verschil
18 dmg_evo = '0.08'; %van 0.2 naar 0.1. Maakt ook geen
19   verschil. 0.4 ook niet. 1 is slecht, 0.05 ook.
20 dmg_stab = '0.001'; %van 0.001 naar 0.005 maakt geen
21   verschil. naar 0.01 is zelfs slechter
22
23 N_el = length(ang_samp3);
24
25 % Pre-allocate cells for input texts
26 text_elset = cell(2*N_el, 1); % Each *Elset
27   definition is 2 lines
28 text_section = cell(7*N_el, 1); % Each **Section 7
29   lines
30 text_mat = cell(9*N_el, 1); % Each *Material 9
31   lines
32
33 for ii = 1:N_el
34   % Store current element number as a string
35   el_no = num2str(ang_samp3(ii,1));
36
37   % Compute endpoint for a unit-length orientation
38   vector (used later to
39   % define the fibre orientation)
40   x_orivec = num2str(cosd(ang_samp3(ii,2)));
41   y_orivec = num2str(sind(ang_samp3(ii,2)));
42
43   % Generate lines for *Elset
44   text_elset{2*ii-1} = ['*Elset, elset=PlaqueEl-' el_no
45     ', generate'];
46   text_elset{2*ii} = [' ' el_no ', ' el_no ', 1'];
47
48   % Generate lines for *Material
49   mat_name = ['HGOPlaque-' el_no];
50   % Material definition

```

```

41 text_mat{9*ii-8} = ['*Material, name=' mat_name];
42 %Damage initiation
43 text_mat{9*ii-7} = ['*Damage Initiation, criterion=
    MAXPE'];
44 text_mat{9*ii-6} = [dmg_init];
45 %Damage evo
46 text_mat{9*ii-5} = ['*Damage Evolution, type=ENERGY'
    ];
47 text_mat{9*ii-4} = [dmg_evo];
48 %Damage stabilization
49 text_mat{9*ii-3} = ['*Damage Stabilization'];
50 text_mat{9*ii-2} = [dmg_stab];
51 % Specify HGO model with single fibre family
52 text_mat{9*ii-1} = '*Anisotropic Hyperelastic,
    holzapfel, local direction = 1';
53 % Model Parameters
54 text_mat{9*ii} = [C10 ', ' D ', ' k1 ', ' k2 ', '
    num2str(kap_samp3(ii,2))]; %kap_sig1(ii)
55
56 % Generate lines for **Section and *orientation
57 text_section{7*ii-6} = ['** Section: PlaqueSection_'
    el_no];
58 % Definition of orientation (rectangular CSYS) and 1
    fibre direction
59 text_section{7*ii-5} = ['*orientation, name=
    ori_PlaqueEl_' el_no ...
60 ', local directions=1, System=RECTANGULAR'];
61 % Define the local X-, Y-axis (in terms of global
    system). We define
62 % them to be the same because the fibre orientations
    were defined as
63 % a counterclockwise-positive angle of rotation
    around the Z-axis
64 text_section{7*ii-4} = '1.0,0.0,0.0,0.0,1.0,0.0';
65 % Define the Axis of Rotation (Z in our case)
66 text_section{7*ii-3} = '3,0.0';
67 % Define fibre orientation using an orientation
    vector in local CSYS
68 text_section{7*ii-2} = [x_orivec ', ' y_orivec ', 0'
    ];
69 % Assign the element type, element set, orientation,
    and material to
70 % the section we have defined
71 text_section{7*ii-1} = ['*Solid Section, elset=
    PlaqueEl_' el_no ...
72 ', orientation=ori_PlaqueEl_' el_no ', material='
    mat_name]; % , controls = EC-1 , weg
73 % [<Stress-Strain Thickness>, <# int. points>]
74 text_section{7*ii} = '1.0,';
75 end

```

```

76
77 %% Write the new .inp text file(s) for ABAQUS
78 % Find the rows in the .inp where node/element
    definitions start
79 [start_node, start_element, end_element,
    start_elsetPLAQUE, end_elsetPLAQUE, start_materials,
    end_part] = FindInputSections(input_filename);
80
81 % Write _elset.inp
82 new_elsetfilename = [new_filename(1:end-4) '_FOelsets.inp
    '];
83 fid = fopen(new_elsetfilename, 'wt');
84 for jj = 1:length(text_elset)
85     fprintf(fid, '%s\n', text_elset{jj});
86 end
87 fclose(fid);
88
89 % Write _material.inp
90 new_matfilename = [new_filename(1:end-4) '_FOmaterials.
    inp'];
91 fid = fopen(new_matfilename, 'wt');
92 for kk = 1:length(text_mat)
93     fprintf(fid, '%s\n', text_mat{kk});
94 end
95 fclose(fid);
96
97 % Write _section.inp
98 new_sectionfilename = [new_filename(1:end-4) '_FOsections
    .inp'];
99 fid = fopen(new_sectionfilename, 'wt');
100 for ll = 1:length(text_section)
101     fprintf(fid, '%s\n', text_section{ll});
102 end
103 fclose(fid);
104
105 % Write new_filename.inp
106
107 % Retrieve the original input text
108 fid = fopen(input_filename, 'r');
109 input = textscan(fid, '%s', 'delimiter', '\n');
110 input = input{1};
111 fclose(fid);
112
113 % Retrieve the model name (the 12 is because 'Model name:
    ' is 12
114 % characters long and the name is after it)
115 model_name = input{2}(strfind(input{2}, 'Model')+12:end);
116
117 % Defining the new Job line and the *Include lines
118 new_jobline = ['**Job name: ' new_filename(1:end-4) '

```

```

    Model name: ' model_name];
119 include_elsetline = ['*Include, Input=' new_elsetfilename
    ];
120 include_sectionline = ['*Include, Input='
    new_sectionfilename];
121 include_matline = ['*Include, Input=' new_matfilename];
122
123 % Writing the new input by inserting the *Include lines
124 new_input = [input(1); ...
125             new_jobline; ...
126             input(3:end_elsetPLAQUE-1); ...
127             include_elsetline; ...
128             input(end_elsetPLAQUE:end_part-1); ...
129             include_sectionline; ...
130             input(end_part:start_materials+1); ...
131             include_matline; ...
132             input(start_materials+2:end)];
133
134 % Writing the new_filename.inp text file
135 fid = fopen(new_filename, 'wt');
136 for mm=1:length(new_input)
137     fprintf(fid, '%s\n', new_input{mm});
138 end
139 fclose(fid);

```

References

- [1] R. Ross, “Atherosclerosis—an inflammatory disease,” *New England journal of medicine*, vol. 340, no. 2, pp. 115–126, 1999.
- [2] R. Virmani, F. D. Kolodgie, A. P. Burke, A. Farb, and S. M. Schwartz, “Lessons from sudden coronary death: a comprehensive morphological classification scheme for atherosclerotic lesions,” *Arteriosclerosis, thrombosis, and vascular biology*, vol. 20, no. 5, pp. 1262–1275, 2000.
- [3] P. Libby, “Atherosclerosis: the new view,” *Scientific American*, vol. 286, no. 5, pp. 46–55, 2002.
- [4] I.-K. Jang, G. J. Tearney, B. MacNeill, M. Takano, F. Moselewski, N. Ifitima, M. Shishkov, S. Houser, H. T. Aretz, E. F. Halpern, *et al.*, “In vivo characterization of coronary atherosclerotic plaque by use of optical coherence tomography,” *Circulation*, vol. 111, no. 12, pp. 1551–1555, 2005.
- [5] K. Sakakura, M. Nakano, F. Otsuka, E. Ladich, F. D. Kolodgie, and R. Virmani, “Pathophysiology of atherosclerosis plaque progression,” *Heart, Lung and Circulation*, vol. 22, no. 6, pp. 399–411, 2013.
- [6] A. C. Akyildiz, L. Speelman, and F. J. Gijssen, “Mechanical properties of human atherosclerotic intima tissue,” *Journal of biomechanics*, vol. 47, no. 4, pp. 773–783, 2014.
- [7] U. Sadat, Z. Teng, V. E. Young, Z. Y. Li, and J. H. Gillard, “Utility of magnetic resonance imaging-based finite element analysis for the biomechanical stress analysis of hemorrhagic and non-hemorrhagic carotid plaques,” *Circulation Journal*, pp. 1101281089–1101281089, 2011.
- [8] U. Sadat, Z. Teng, and J. H. Gillard, “Biomechanical structural stresses of atherosclerotic plaques,” *Expert review of cardiovascular therapy*, vol. 8, no. 10, pp. 1469–1481, 2010.
- [9] T. Wissing, S. Serra, K. Van der Heiden, A. Smits, C. Bouten, and F. Gijssen, “A tissue engineered collagenous fibrous cap model to systematically elucidate atherosclerotic plaque rupture,” 2021.
- [10] G. A. Holzapfel and R. W. Ogden, “A damage model for collagen fibres with an application to collagenous soft tissues,” *Proceedings of the Royal Society A*, vol. 476, no. 2236, p. 20190821, 2020.
- [11] T. C. Gasser, R. W. Ogden, and G. A. Holzapfel, “Hyperelastic modelling of arterial layers with distributed collagen fibre orientations,” *Journal of the royal society interface*, vol. 3, no. 6, pp. 15–35, 2006.
- [12] D. R. Nolan, A. L. Gower, M. Destrade, R. W. Ogden, and J. McGarry, “A robust anisotropic hyperelastic formulation for the modelling of soft tissue,” *Journal of the mechanical behavior of biomedical materials*, vol. 39, pp. 48–60, 2014.
- [13] A. G. Holzapfel, “Nonlinear solid mechanics ii,” 2000.

- [14] E. E. van Haaften, T. B. Wissing, M. C. Rutten, J. A. Bulsink, K. Gashi, M. A. van Kelle, A. I. Smits, C. V. Bouten, and N. A. Kurniawan, “Decoupling the effect of shear stress and stretch on tissue growth and remodeling in a vascular graft,” *Tissue Engineering Part C: Methods*, vol. 24, no. 7, pp. 418–429, 2018.
- [15] “Reduced integration in finite element analysis.”
- [16] J. M. Melenk and I. Babuška, “The partition of unity finite element method: basic theory and applications,” *Computer methods in applied mechanics and engineering*, vol. 139, no. 1-4, pp. 289–314, 1996.
- [17] O. Gültekin, H. Dal, and G. A. Holzapfel, “A phase-field approach to model fracture of arterial walls: theory and finite element analysis,” *Computer methods in applied mechanics and engineering*, vol. 312, pp. 542–566, 2016.
- [18] A. Natali, P. Pavan, E. Carniel, M. Lucisano, and G. Tagliavero, “Anisotropic elasto-damage constitutive model for the biomechanical analysis of tendons,” *Medical engineering & physics*, vol. 27, no. 3, pp. 209–214, 2005.
- [19] B. Calvo, E. Peña, M. Martinez, and M. Doblaré, “An uncoupled directional damage model for fibred biological soft tissues. formulation and computational aspects,” *International journal for numerical methods in engineering*, vol. 69, no. 10, pp. 2036–2057, 2007.
- [20] N. Driessen, W. Wilson, C. Bouten, and F. Baaijens, “A computational model for collagen fibre remodelling in the arterial wall,” *Journal of theoretical biology*, vol. 226, no. 1, pp. 53–64, 2004.
- [21] S. W. Tsai and E. M. Wu, “A general theory of strength for anisotropic materials,” *Journal of composite materials*, vol. 5, no. 1, pp. 58–80, 1971.